

POLITECNICO DI TORINO

Master of Science Degree in Automotive Engineering

Master Thesis

**Mathematical Application on Optimizing Comfort
Performance of Ambulance**



Supervisor:

Prof. Marcello Delitala

Candidate:

Chang Jiaming

Academic Year 2021-2022

Acknowledgement

I would like to express my deep gratitude to Professor Marcello Delitala, for giving me this amazing chance to work on this project. In every virtual meeting, his patient guidance and encouragements give me a lot of confidence. Every time he gives me feedback and guidance of the work as soon as possible. All of his encouragement and kindness will motivates me after I graduate in the future days.

CONTENTS:

1. Introduction.....	3
2. 7 DOF Truck Model.....	7
2.1 Building of Mathematical Model.....	7
2.2 Truksim Model.....	10
2.2.1 TruckSim model of the vehicle.....	10
2.2.2 TruckSim model of the bumps.....	11
2.3 Simulate the Mathematical Model.....	11
2.4 Comparison of Simulink model and Truksim model.....	12
3. 8 DOF Ambulance Model.....	15
3.1 Mathematical Model.....	16
3.1.1 Ambulance Model.....	16
3.1.2 Dynamic Equations of Each Degrees of Freedom.....	16
3.1.3 Ambulance Parameters.....	19
3.1.4 Parameter Optimization and Analysis.....	19
3.2 Simulation and Results.....	20
3.2.1 Simulation of the sinusoidal road profile.....	20
3.2.2 8-DOF Simulink model.....	21
3.2.3 Choosing the Optimum k_b and c_b (point “2”).....	21
3.2.4 Choosing the Optimum k_b and c_b (point “1”).....	25
3.3 Simulation of Grade C Road Profile.....	27
4. Confirm Optimal k_b and c_b.....	29
4.1 Influence of k_b and c_b to Comfort of the Patient.....	29
4.1.1 RMS value of the signal.....	29
4.1.2 RMS value of \ddot{z}_b varying k_b	30

4.1.3 RMS value of \ddot{z}_b varying c_b	31
4.1.4 Responses of the system based on optimum value of k_b and c_b	31
4.2 Influence of Speed of Ambulance to the Results.....	32
4.2.1 Influence of different speed on comfort of the patients.....	33
4.2.2 Influence of different speed on choosing optimum and c_b	35
4.3 Comparison Between Sinusoidal and Random Road Profile.....	36
5. HIS Ambulance Model.....	37
5.1 Working Principle of HIS Suspension.....	37
5.2 Mathematical Model of HIS Subsystem.....	39
5.3 Integration of Ambulance Model and HIS Suspension Model.....	42
5.3.1 Stiffness matrix K_{HIS}	42
5.3.2 Damping matrix C_{HIS}	43
5.4 Optimize the Parameters of HIS System for the Ambulance Model.....	43
5.4.1 Indicators of comfort performance of the ambulance.....	43
5.4.2 Simulink model of the integrated model.....	44
5.4.3 Find the optimized value of μ	44
5.4.4 Find the optimized value of η_i	45
5.5 Comparison Between HIS and Conventional Suspension.....	47
6. Conclusion.....	51
Bibliography.....	53

Chapter 1

Introduction

The good comfort performance of the vehicle is a very important requirement for most of the vehicles, particularly for ambulance ^[1]. To evaluate this performance, however, the experimental on field is expensive and inconvenient and by using experimental data, it is not possible to analyse the performance of the vehicle or adjust the parameters during the design phase of the produce. But by using mathematical modeling of the vehicle, the virtual results of the performance can be simulated by Matlab/Simulink before the manufacture of the vehicle, and if the mathematical model is made correctly, the simulation results are also relatively accurate. By looking at the results of the simulation, evaluation can be made which is also a much more convenient way. So in the first part of the thesis, a 7 DOF full vehicle mathematical is built and the simulation results are compared to experimental data from Trucksim. In this way, the accuracy of our mathematical model is confirmed.

In addition, the comfort performance of the ambulance is particularly analyzed. When the ambulance is riding on the road, to carry the patients to the hospital as soon as possible, the velocity of the ambulance is often very high. But the vibration and instability experienced in an ambulance can lead to secondary injury to a patient and discourage a paramedic from emergency care ^[2]. So good comfort performance also is very important as well as the requirement for the speed of the ambulance ^[3]. But the reality is that ambulances are usually customized or adapted from cargo transport vehicles, such as trucks or vans. Patients transported by these vehicles are exposed to severe accelerations, particularly due to braking, in curves, and by driving over obstacles or uneven pavements. The vibration produced when an ambulance drives over an uneven surface can affect the vital functions of the human body (cardiovascular system, skeleton, central nervous system, respiratory system), being harmful to the already delicate clinical condition of the patient ^[5]. Patients transported in recumbent position are more sensitive to vertical vibrations when compared to a

passenger in a standing or seated position ^[6]. In addition, vibration of the human body is most uncomfortable for sick or injured patients.

So, to improve the comfort of the lying patient in this case, there are two ways: to adjust the suspension of the ambulance to be very soft or to properly design the stretcher suspension (the suspension between the stretcher and the vehicle body). But since the truck like ambulance is driving at relatively higher speed than regular trucks, and the road profile and the traffic conditions are usually unpredictable. The ambulance is likely to rollover during cornering at this high speed or during riding at bad quality road. So the handling requirement of ambulance is higher than regular trucks. But to give the ambulance good handling we need to make the suspension stiffer which unavoidably sacrifices the comfort performance. In this case, the first is not applicable. So, to improve the comfort performance of the patients, the better method is to properly design the stretcher suspension. We can do this by correctly choosing the stiffness and damping value of the stretcher suspension. So, the second mathematical model built is the 8 DOF ambulance model.

For ambulances, ride comfort, roll- and pitch-resistant performance requirements are more demanding than passenger cars. Particularly, the roll-resistant moment and pitch resistant moments of the pitch–roll-resistant HIS are coupled together and there is a trade off among ride comfort, roll, and pitch dynamics. For example, the optimal roll-resistant performance of the vehicle is usually accompanied with excessive pitch-resistant moment, which would decrease the ride comfort of the vehicle. On the other hand, increasing the ride comfort would reduce the roll- and pitch-resistant performance. Therefore, the ride comfort, roll resistance, and pitch resistance trade off analysis and parameter design approach for Hydraulic Interconnected Suspension (HIS) are conducted in this thesis to balance these characters to achieve an overall optimal performance of the ambulance. This thesis presents a HIS system to improve stability and attenuate vibration for both lying patients and paramedics. This new suspension system can achieve enhanced cooperative control of the bounce and pitch/roll motion-modes for the ambulance. The key for improving comprehensive dynamic performance is to properly assign the bounce, pitch, and roll mode stiffness by parameter design of HIS system. So, the third model in this thesis is integrated ambulance and HIS mathematical model.

In general, this thesis built three mathematical models in total.

1. 7 DOF full vehicle model
2. 8 DOF ambulance model
3. Integrated HIS ambulance model

For the first model, the whole vehicle can be regarded as two parts: sprung mass and unsprung mass. Since in this thesis the independent suspension is used, there are four unsprung masses representing the four wheels. Between sprung mass and each of the unsprung mass connected by compliance components: a spring and a damper. And between the road excitation and each of the four wheels the compliance are represented by a spring. The degrees of freedom for sprung mass are rolling, pitching and heave motion. The degrees of freedom for each of the unsprung mass is only heave motion. So there are 7 DOF in total. The road excitation of the input is Left/Right bumper. Based on this scheme, referring to each of 7 DOF, the Newton law is applied and the second order differential equations are written. In this way, the 7 DOF mathematical model is built. Once this model is built, to verify the accuracy of the model, the simulations of the comfort responses are compared with the experimental data from the Trucksim which shares the same values of all of the parameters with mathematical model. This part will be discussed in Chapter 2.

For the second model (ambulance model), based on the first model, an additional mass which represents the total masses of patient and stretcher is added onto the sprung mass. The compliance between this additional mass and sprung mass (stretcher suspension) are consists of two parts: one spring and one damper. This additional mass has one degree of freedom: heave motion. So this new ambulance model has 8 DOF. To improve the comfort responses of the patient, the key parameters that need to be properly designed are stiffness and damping values of the stretcher suspension. In terms of road excitation of input of this model, a sinusoidal and grade C random road profile is used respectively. Then the stiffness and damping values of the stretcher suspension are varied and RMS values of vertical accelerations of patients and vehicle body at each of the varied values are compared. By comparing the results, the optimum parameters of stretcher suspension are found. Furthermore, the influences of variation of ambulance speeds and different roads excitation on choosing optimum stiffness and damping values of stretcher suspension are also analyzed. This part will be discussed in Chapter 3 and Chapter 4.

For the third model in this thesis. The conventional suspension between sprung and unsprung mass is replaced with Hydraulic Interconnected Suspension (HIS) to further improve the comfort performance of the ambulance. The mathematical model of HIS suspension is built and coupled together with 8 DOF ambulance model forming a new dynamic model. Then based on this new model, the RMS values of acceleration of vertical motion of sprung mass and patient, the pitch motion and roll motion of the sprung mass are used as the indicators of the comfort performance of the ambulance. Then, the key parameters of the HIS suspension are varied in order to find their optimum value corresponding to the best trade off between each indicators and achieve an overall optimal performance of the ambulance. In the end, based on these optimum parameters, the comfort performance of ambulance with HIS suspension is

compared with conventional suspension to verify our conclusion. This part will be discussed in Chapter 5.

Based on the integrated HIS ambulance model, the accelerations and displacements of vertical motions of patient and sprung mass, the pitch and roll motions of sprung mass are output in time domain and compared with the ambulance model with conventional suspension. The result is that the comfort performance is largely improved.

Chapter 2

7 DOF Truck Model

Following ^[7], in this chapter we propose a 7 DOF full car mathematical model.

This model consists of a sprung mass and four unsprung masses represented by four wheels. Between sprung mass and unsprung masses are compliance represented by spring and damper. Between unsprung masses and the ground are just the stiffness of the tire ignoring the damping of the tire. The sprung mass has 3-degree of freedom representing body bounce (Z_s), roll (ϕ) and pitch (θ) movement, while the unsprung masses have 4-degree of freedom in vertical motions (Z_{u_f1} , Z_{u_f2} , Z_{u_r1} , Z_{u_r2}). We choose a compact truck and find the relevant data in Trucksim. Based on these data, we build the 7 DOF mathematical model and calculate the differential equations of each 7 DOF variables. Then we output the bounce (Z_s), roll (ϕ) and pitch (θ) motions of the vehicle body and compare the results with the plot from Trucksim to verify the accuracy of our mathematical model.

2.1 Building of Mathematical Model

In this model, the vehicle aerodynamic effect is neglected and the road is assumed to be level except for road disturbance. Based on the 7 DOF model in Figure 2.1

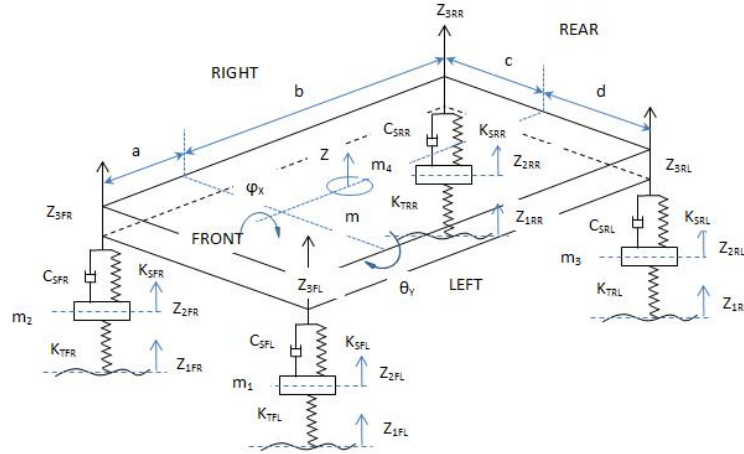


Figure 2.1 7 DOF full vehicle model

The displacement of sprung mass can be calculated as (Where m_s is the sprung mass of the vehicle, \ddot{z}_s is the acceleration of sprung mass. F represent the force. In the sub note, S for spring, D for damper, F for front, R for rear, L for left, R for right):

$$m_s \ddot{z}_s = -F_{SFL} - F_{DFL} - F_{SFR} - F_{DFR} - F_{SRL} - F_{DRL} - F_{SRR} - F_{DRR}$$

Acceleration at unsprung masses can be given by (Where m_u represent the unsprung mass and T for tire):

$$\begin{cases} m_{u_fr} \cdot \ddot{z}_{u_fr} = F_{SFR} + F_{DFR} - F_{TFR} \\ m_{u_fl} \cdot \ddot{z}_{u_fl} = F_{SFL} + F_{DFL} - F_{TFL} \\ m_{u_rr} \cdot \ddot{z}_{u_rr} = F_{SRR} + F_{DRR} - F_{TRR} \\ m_{u_rl} \cdot \ddot{z}_{u_rl} = F_{SRL} + F_{DRL} - F_{TRL} \end{cases}$$

The pitch motion of the sprung mass θ can be given by (where J_y is the moment of inertia about y axis, a is the distance between front axle and center of gravity, b is the distance between rear axle and center of gravity):

$$J_y \ddot{\theta} = -(F_{SFL} + F_{DFL} + F_{SFR} + F_{DFR}) \cdot a + (F_{SRL} + F_{DRL} + F_{SRR} + F_{DRR}) \cdot b$$

The roll motion of the sprung mass can be given by (where J_x is the moment of inertia about x axis and t represent the wheel track):

$$J_x \ddot{\phi} = -(F_{SFL} + F_{DFL} + F_{SRL} + F_{DRL}) \cdot t + (F_{SFR} + F_{DFR} + F_{SRR} + F_{DRR}) \cdot t$$

Represent the all the forces with stiffness k and damping c , these seven equations can be given by:

Sprung mass:

$$m_s \ddot{z}_s = -k_{sf}(z_{s_fl} - z_{u_fl}) - c_{sf}(\dot{z}_{s_fl} - \dot{z}_{u_fl}) - k_{sf}(z_{s_fr} - z_{u_fr}) - c_{sf}(\dot{z}_{s_fr} - \dot{z}_{u_fr}) - k_{rf}(z_{s_rl} - z_{u_rl}) - c_{sr}(\dot{z}_{s_rl} - \dot{z}_{u_rl}) - k_{sr}(z_{s_rr} - z_{u_rr}) - c_{sr}(\dot{z}_{s_rr} - \dot{z}_{u_rr})$$

$$J_y \ddot{\theta} = -\left[k_{sf}(z_{s_fl} - z_{u_fl}) + c_{sf}(\dot{z}_{s_fl} - \dot{z}_{u_fl}) + k_{sf}(z_{s_fr} - z_{u_fr}) + c_{sf}(\dot{z}_{s_fr} - \dot{z}_{u_fr}) \right] \cdot a + \left[k_{sr}(z_{s_rl} - z_{u_rl}) + c_{sr}(\dot{z}_{s_rl} - \dot{z}_{u_rl}) + k_{sr}(z_{s_rr} - z_{u_rr}) + c_{sr}(\dot{z}_{s_rr} - \dot{z}_{u_rr}) \right] \cdot b$$

$$J_x \ddot{\phi} = -\left[k_{sf}(z_{s_fl} - z_{u_fl}) + c_{sf}(\dot{z}_{s_fl} - \dot{z}_{u_fl}) + k_{sr}(z_{s_rl} - z_{u_rl}) + c_{sr}(\dot{z}_{s_rl} - \dot{z}_{u_rl}) \right] \cdot t + \left[k_{sr}(z_{s_fr} - z_{u_fr}) + c_{sf}(\dot{z}_{s_fr} - \dot{z}_{u_fr}) + k_{sr}(z_{s_rr} - z_{u_rr}) + c_{sr}(\dot{z}_{s_rr} - \dot{z}_{u_rr}) \right] \cdot t$$

Unsprung mass:

$$m_{u_fr} \cdot \ddot{z}_{u_fr} = k_{sf}(z_{s_fr} - z_{u_fr}) + c_{sf}(\dot{z}_{s_fr} - \dot{z}_{u_fr}) - k_t(z_{u_fr} - h_{fr})$$

$$m_{u_fl} \cdot \ddot{z}_{u_fl} = k_{sf}(z_{s_fl} - z_{u_fl}) + c_{sf}(\dot{z}_{s_fl} - \dot{z}_{u_fl}) - k_t(z_{u_fl} - h_{fl})$$

$$m_{u_rr} \cdot \ddot{z}_{u_rr} = k_{sr}(z_{s_rr} - z_{u_rr}) + c_{sr}(\dot{z}_{s_rr} - \dot{z}_{u_rr}) - k_t(z_{u_rr} - h_{rr})$$

$$m_{u_rl} \cdot \ddot{z}_{u_rl} = k_{sf}(z_{s_rl} - z_{u_rl}) + c_{sr}(\dot{z}_{s_rl} - \dot{z}_{u_rl}) - k_t(z_{u_rl} - h_{rl})$$

Rearranging these seven equations, the second order differential equations of this 7 DOF model can be given as (Where $X = \{z_s \ \theta \ \varphi \ z_{u_fl} \ z_{u_fr} \ z_{u_rl} \ z_{u_rr}\}^T$):

$$M \cdot \ddot{X} + C \cdot \dot{X} + K \cdot X = F$$

In detail, M, C, K and F can be given as:

$$M = \begin{bmatrix} m_s & 0 & 0 & 0 & 0 & 0 & 0 \\ 0 & J_y & 0 & 0 & 0 & 0 & 0 \\ 0 & 0 & J_x & 0 & 0 & 0 & 0 \\ 0 & 0 & 0 & m_{u_fl} & 0 & 0 & 0 \\ 0 & 0 & 0 & 0 & m_{u_fr} & 0 & 0 \\ 0 & 0 & 0 & 0 & 0 & m_{u_rl} & 0 \\ 0 & 0 & 0 & 0 & 0 & 0 & m_{u_rr} \end{bmatrix}$$

$$K = \begin{bmatrix} 2(k_{sf} + k_{sr}) & 2(bk_{sr} - ak_{sf}) & 0 & -k_{sf} & -k_{sf} & -k_{sr} & -k_{sr} \\ 2(bk_{sr} - ak_{sf}) & 2(a^2k_{sf} + b^2k_{sr}) & 0 & ak_{sf} & ak_{sf} & -bk_{sr} & -bk_{sr} \\ 0 & 0 & 2(t^2k_{sf} + t^2k_{sr}) & -tk_{sf} & tk_{sf} & -tk_{sr} & tk_{sr} \\ -k_{sf} & ak_{sf} & -tk_{sf} & k_{sf} + k_t & 0 & 0 & 0 \\ -k_{sf} & ak_{sf} & tk_{sf} & 0 & k_{sf} + k_t & 0 & 0 \\ -k_{sr} & -bk_{sr} & -tk_{sr} & 0 & 0 & k_{sr} + k_t & 0 \\ -k_{sr} & -bk_{sr} & tk_{sr} & 0 & 0 & 0 & k_{sr} + k_t \end{bmatrix}$$

$$C = \begin{bmatrix} 2(c_{sf} + c_{sr}) & 2(bc_{sr} - ac_{sf}) & 0 & -c_{sf} & -c_{sf} & -c_{sr} & -c_{sr} \\ 2(bc_{sr} - ak_{sf}) & 2(a^2c_{sf} + b^2c_{sr}) & 0 & ac_{sf} & ac_{sf} & -bc_{sr} & -bc_{sr} \\ 0 & 0 & 2(t^2c_{sf} + t^2c_{sr}) & -tc_{sf} & tc_{sf} & -tc_{sr} & tc_{sr} \\ -c_{sf} & ac_{sf} & -tc_{sf} & c_{sf} & 0 & 0 & 0 \\ -c_{sf} & ac_{sf} & tc_{sf} & 0 & c_{sf} & 0 & 0 \\ -c_{sr} & -bc_{sr} & -tc_{sr} & 0 & 0 & c_{sr} & 0 \\ -c_{sr} & -bc_{sr} & tc_{sr} & 0 & 0 & 0 & c_{sr} \end{bmatrix}$$

$$F = \{0 \quad 0 \quad 0 \quad k_t h_{fl} \quad k_t h_{fr} \quad k_t h_{rl} \quad k_t h_{rr}\}^T$$

We will further use this model in Simulink to have the numerical results.

2.2 Trucksim Model

2.2.1 TruckSim model of the vehicle

TruckSim is used to obtain the relevant parameters of this data and verify the accuracy of this mathematical model. The relevant parameters is based on a compact truck given by TruckSim. The detail of the data is shown in figures below.

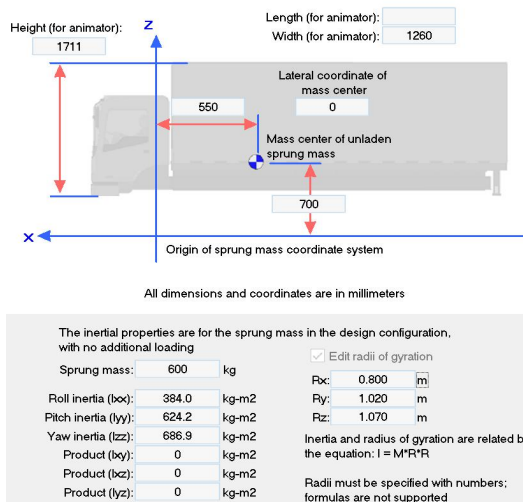


Figure 2.1 Sprung mass parameters

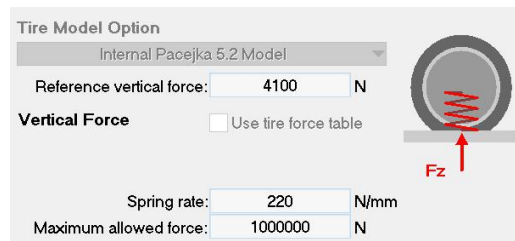


Figure 2.2 Unsprung mass parameters

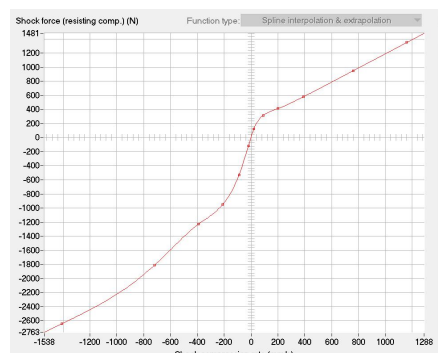
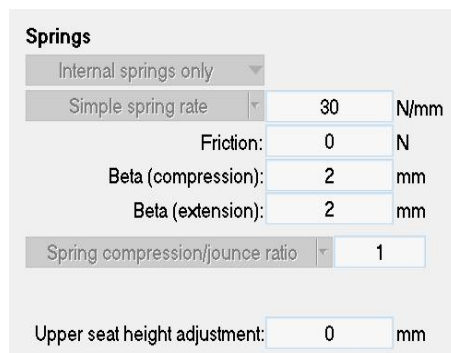


Figure 2.3 Front axle parameters

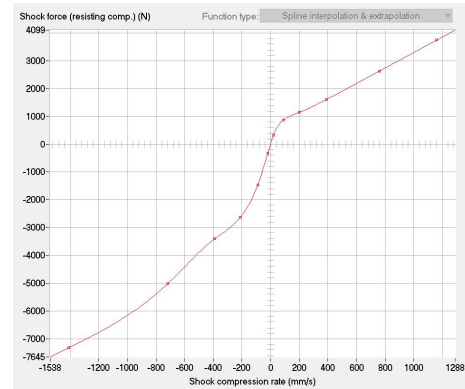
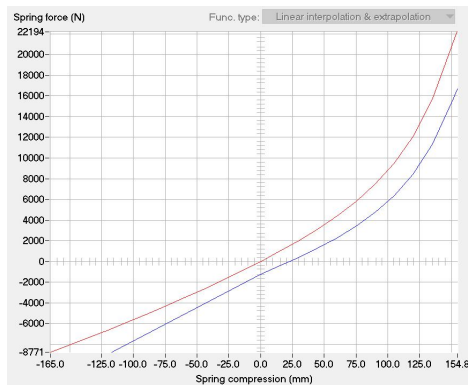


Figure 2.4 Rear axle parameters

All of the parameters we need are summarized in the Table 2.1

Table 2.1 Parameters of 7 DOF model

Notation	Values	Units	Notation	Values	Units
m_s	600	kg	k_t	220000	N/m
J_y	624.2	Kg*m2	c_{sf}	5200	N*s/m
J_x	384	Kg*m2	c_{sr}	5200	N*s/m
m_u	105	kg	a	0.55	m
k_{sf}	15000	N/m	l	1.925	m
k_{sr}	31000	N/m	t	0.63	m

2.2.2 TruckSim model of the bumps

To use TruckSim to verify the results of Simulink obtained from the mathematical model, we let the vehicle running across the left/right bumps. The 3D and 2D profiles are shown in figure 3.5. During this procedure, the speed of the vehicle is 8 km/h. The vehicle start at station 100 m shown in the 2D profile and the bump starts at station 109 m and ends at station 121 m. This whole procedure takes about 14 seconds covering 30 m. The length and width of each bump is 6 m and the height of each bump is 0.1 m.

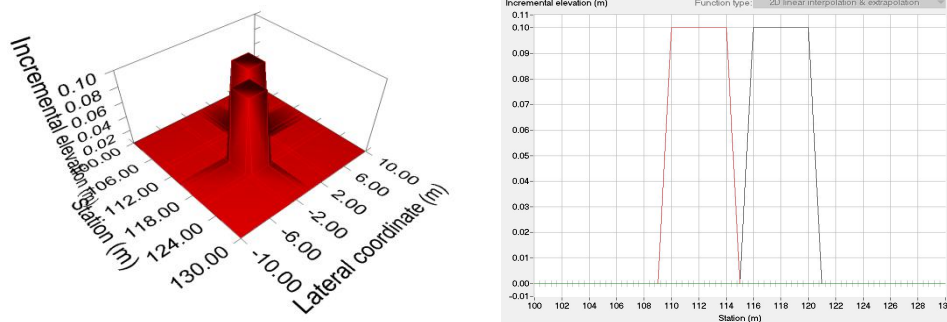


Figure 3.5 3D and 2D profiles of the bumps

2.3 Simulate the Mathematical Model

Based on the second order differential equations, the Simulink block diagram model can be built shown in Figure 2.5. (we plus 0.05 to Z_s Trucksim data to offset the vertical displacement caused by the weight of the vehicle)

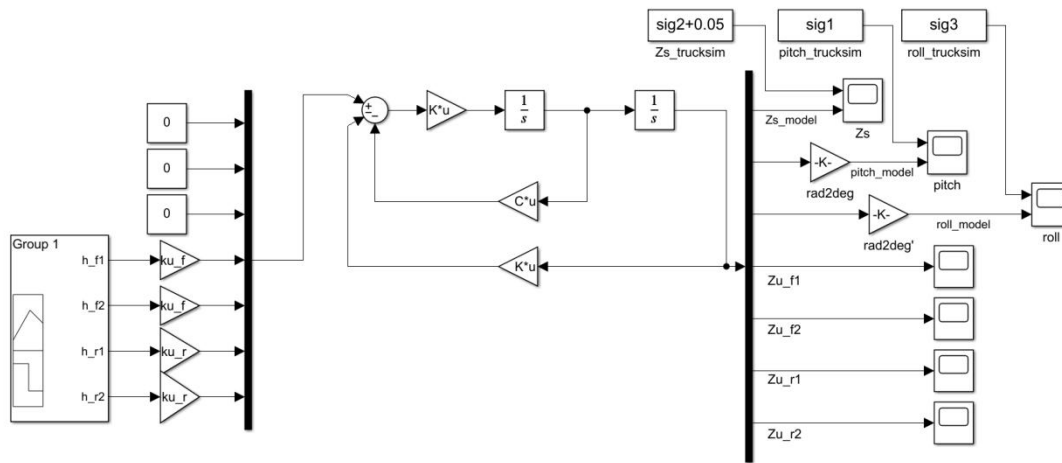


Figure 2.5 7 DOF Simulink Model

In this Simulink model, the four input signals are h_{fr} , h_{rl} , h_{fl} , h_{fr} . The signal builder is used to draw the profiles of these four inputs. The profiles are shown in Figure 2.6.

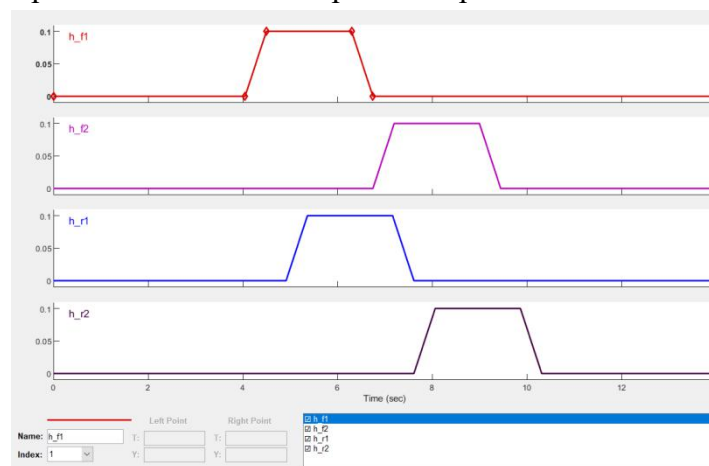


Figure 2.6 Profiles of the bumps in Simulink

2.4 Comparison of Simulink model and Trucksim model

Running the Simulink model and compares the result with data collected in Trucksim, we have these figures. Figure 2.7 and 2.8 show the Simulink and Trucksim simulation of roll (ϕ) and pitch (θ) performances (the unit is deg), which have the similar trend but slightly differences in magnitude. Figure 2.9 shows the simulation result of Simulink sprung mass vertical displacement (z_s) which has the same trend but some differences in magnitude (the unit is m). The error maybe due to simplified model used in Simulink, while Trucksim model that is based on actual tested vehicle simulation process thus becomes more precise.

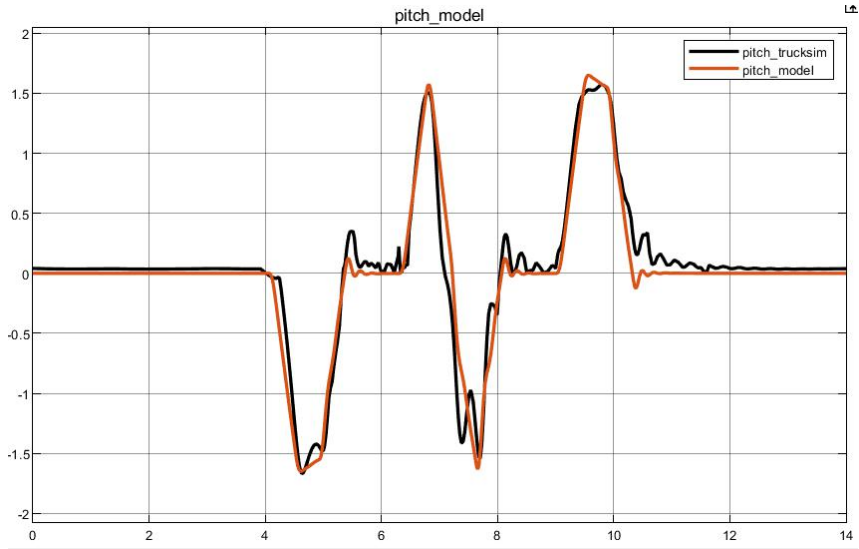


Figure 2.7 Comparison of pitch motion

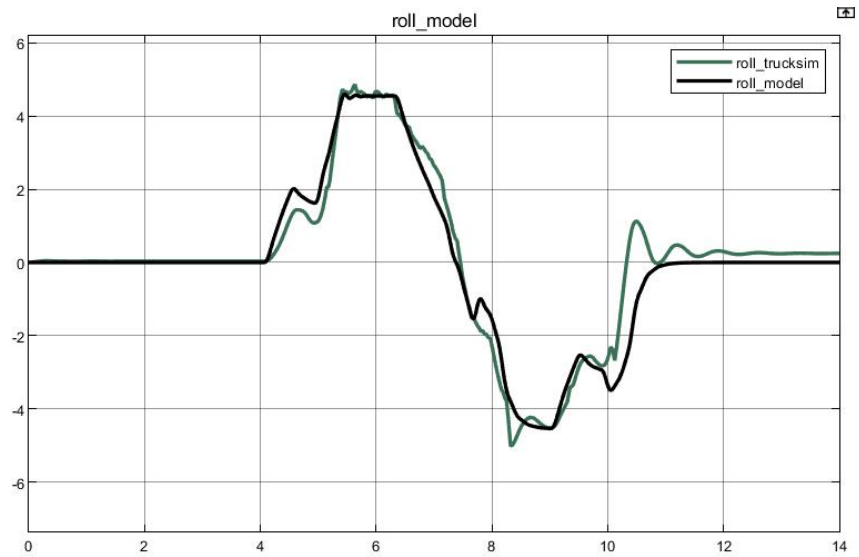


Figure 2.8 Comparison of roll motion

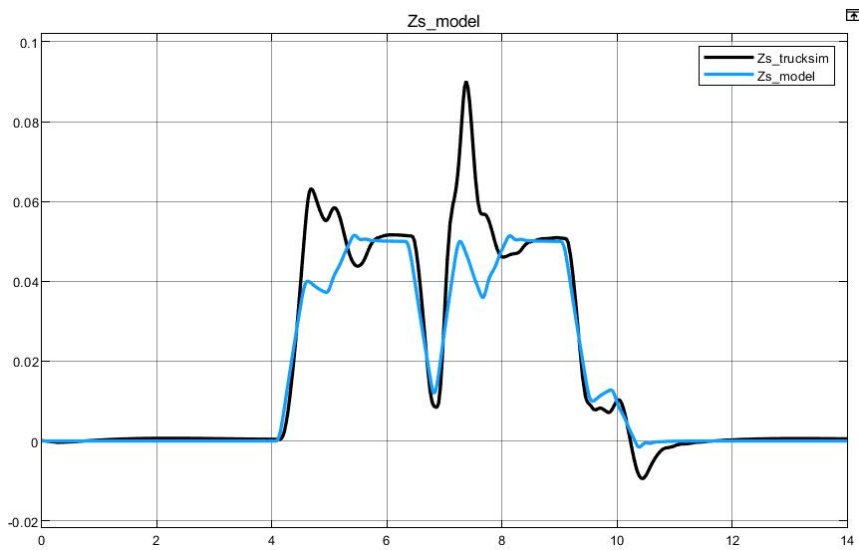


Figure 2.9 Comparison of sprung mass vertical displacement

In conclusion, since we made a lot of simplification when building this mathematical model, like we neglect the aerodynamic effect of the vehicle and so on, but we still get the similar result as Trucksim. So, we can basically ensure the accuracy of our mathematical model.

Chapter 3

8 DOF Ambulance Model

Following ^[8], in this chapter we propose a 8 DOF ambulance model.

Most ambulances are customized or adapted from cargo transport vehicles like trucks, and these vehicles are usually heavier and less comfortable than passenger cars. In this case, the passenger on ambulance will subject to severe acceleration during braking, curves or running on a uneven road. But the patients in ambulances are usually exposed to serious illness or injury, any severe acceleration can cause damage to the body of patients. Particularly, patients in lying down position are more sensitive to vertical acceleration when comparing to a passenger in standing or seated position. In this case, to improve the comfort performance of the patients, we can either focus on properly designing the suspension of the ambulance or the suspension of the stretch.

But since the ambulance is driving at relatively higher speed than regular trucks, the ambulance is likely to rollover during cornering at this high speed. So the handling requirement of ambulance is higher than regular trucks. But to give the ambulance good handling we need to make the suspension stiffer. So, to make the patients more comfortable and at the same time not affecting the handling performance of the ambulance, we focus on properly designing the suspension of the stretch.

There are many ways of designing the suspension of the stretch. In this thesis, we focus on properly choosing the stiffness and damping value of the suspension to achieve the minimum vertical displacement and acceleration of the stretch. To do this, a mathematical model is built and a sinusoidal shape of the road profile is used as the input signal of the system. Then different set of stiffness and damping value (k_b and c_b) is tested to find the optimum k_b and c_b . With this optimum value, we output the vertical displacement, roll angle, pitch angle and acceleration of the ambulance during

the riding on the sinusoidal road. In the end, we used the grade C road profile to verify the optimum k_b and c_b also applied to the real case.

3.1 Mathematical Model

3.1.1 Ambulance Model

Including the stretcher, the 8 DOF dynamic model is built shown in Figure 3.1(a). The 8 DOF are vertical motion of the stretcher (z_b), roll motion, pitch motion and vertical motion of the sprung mass (φ , θ and z_s), and vertical motions of four unsprung mass (z_{fl} , z_{fr} , z_{rr} , z_{rl}). The compliance between stretcher and sprung mass is modeled by spring stiffness k_b and damping value c_b . The compliance between sprung and unsprung mass is modeled as spring stiffness k_{fr} , k_{fl} , k_{rr} , k_{rl} and damping value c_{fr} , c_{fl} , c_{rr} , c_{rl} . The compliance of each tire is modeled as k_{tfl} , k_{tfr} , k_{trr} , k_{trl} and c_{tfl} , c_{tfr} , c_{trr} , c_{trl} . The most critical region of the patient are head and stomach shown as point 2 and point 1 in Figure 3.1(b). These two points will be analysed respectively which define the position of mb (x_b and y_b).

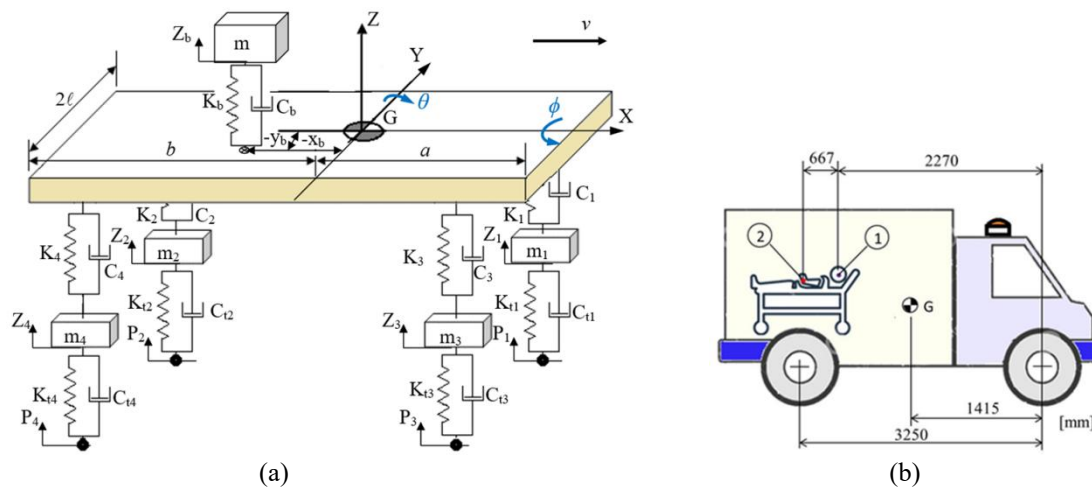


Figure 3.1 (a) 8 DOF ambulance model (b) Locations of point 1 and 2

Sinusoidal Road Profile:

The sinusoidal shape of road profile consists of three successive bumps of height equal to 0.1m with the total length of 19.5m shown in Figure 3.2. The velocity of the ambulance is 30 km/h.

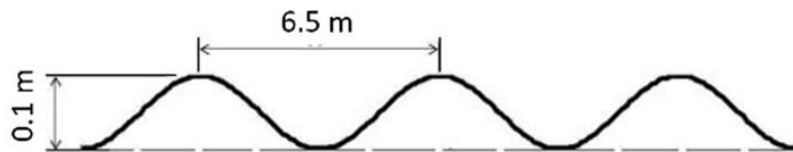


Figure 3.2 Sinusoidal road profile

3.1.2 Dynamic Equations of Each Degrees of Freedom

The equations of motion for this system can be derived according to Newton Law.

The vertical acceleration of m_b is caused by relative vertical motion between m_b and m_s , roll motion and pitch motion of sprung mass:

$$m_b \ddot{z}_b = -(z_b - z_s)k_b - (\dot{z}_b - \dot{z}_s)c_b - k_b \phi \cdot y_b + k_b \theta \cdot x_b - c_b \dot{\phi} \cdot y_b + c_b \dot{\theta} \cdot x_b$$

The vertical acceleration of m_s is caused by relative vertical motion between m_b and m_s , vertical motion of four unsprung masses. In addition, it can be also affected by roll motion and pitch motion of sprung mass:

$$\begin{aligned} m_s \ddot{z}_s = & -(z_s - z_{fl})k_{fl} - (\dot{z}_s - \dot{z}_{fl})c_{fl} - (z_s - z_{fr})k_{fr} - (\dot{z}_s - \dot{z}_{fr})c_{fr} - (z_s - z_{rl})k_{rl} - (\dot{z}_s - \dot{z}_{rl})c_{rl} \\ & - (z_s - z_{rr})k_{rr} - (\dot{z}_s - \dot{z}_{rr})c_{rr} + (bk_{fl} + bk_{fr} - ak_{rl} - ak_{rr})\theta - k_b \theta \cdot y_b + (bc_{fl} + bc_{fr} - ac_{rl} - ac_{rr})\dot{\theta} \\ & - c_b \dot{\theta} \cdot y_b + (lk_{fl} + lk_{rl} - lk_{rr} - lk_{fr})\phi + k_b x_b \phi + (lc_{fl} + lc_{rl} - lc_{rr} - lc_{fr})\dot{\phi} + c_b x_b \dot{\phi} \end{aligned}$$

The acceleration of pitch motion of sprung mass is caused by relative vertical motion between sprung mass and unsprung masses, relative motion between sprung mass and stretcher, and the pitch motion itself. In addition, because of the presence of the asymmetry stretcher, roll motion of sprung mass can also affect the acceleration of pitch motion:

$$\begin{aligned} J_y \ddot{\theta} = & ak_{fl}(z_s - z_{fl}) + ac_{fl}(\dot{z}_s - \dot{z}_{fl}) + ak_{fr}(z_s - z_{fr}) + ac_{fr}(\dot{z}_s - \dot{z}_{fr}) - bk_{rl}(z_s - z_{rl}) - bc_{rl}(\dot{z}_s - \dot{z}_{rl}) \\ & - bk_{rr}(z_s - z_{rr}) - bc_{rr}(\dot{z}_s - \dot{z}_{rr}) + x_b k_b (z_b - z_s) + x_b c_b (\dot{z}_b - \dot{z}_s) - k_{fr} \theta \cdot a^2 - k_{fl} \theta \cdot a^2 - k_{rr} \theta \cdot b^2 \\ & - k_{rl} \theta \cdot b^2 - k_b \theta \cdot x_b^2 + k_b \phi \cdot y_b x_b - c_{fr} \dot{\theta} \cdot a^2 - c_{fl} \dot{\theta} \cdot a^2 - c_{rr} \dot{\theta} \cdot b^2 - c_{rl} \dot{\theta} \cdot b^2 - c_b \dot{\theta} \cdot x_b^2 + c_b \dot{\phi} \cdot y_b x_b \end{aligned}$$

In the same way we can calculate the acceleration of roll motion of the sprung mass:

$$\begin{aligned} J_x \ddot{\phi} = & -lk_{fl}(z_s - z_{fl}) - lc_{fl}(\dot{z}_s - \dot{z}_{fl}) - lk_{rl}(z_s - z_{rl}) - lc_{rl}(\dot{z}_s - \dot{z}_{rl}) + lk_{fr}(z_s - z_{fr}) + lc_{fr}(\dot{z}_s - \dot{z}_{fr}) \\ & + lk_{rr}(z_s - z_{rr}) + lc_{rr}(\dot{z}_s - \dot{z}_{rr}) - y_b k_b (z_b - z_s) + y_b c_b (\dot{z}_b - \dot{z}_s) - k_{fr} \phi \cdot l^2 - k_{fl} \phi \cdot l^2 - k_{rr} \phi \cdot l^2 \\ & - k_{rl} \phi \cdot l^2 - k_b \phi \cdot y_b^2 + k_b \theta \cdot x_b y_b - c_{fr} \dot{\phi} \cdot l^2 - c_{fl} \dot{\phi} \cdot l^2 - c_{rr} \dot{\phi} \cdot l^2 - c_{rl} \dot{\phi} \cdot l^2 - c_b \dot{\phi} \cdot y_b^2 + c_b \dot{\theta} \cdot x_b y_b \end{aligned}$$

The vertical acceleration of unsprung mass is caused by relative motion between sprung and unsprung mass, roll and pitch motion of sprung mass and the road excitation:

$$\begin{aligned} m_{fl} \ddot{z}_{fl} = & k_{fl} z_s + c_{fl} \dot{z}_s + (-k_{fl} - k_{yfl}) z_{fl} + (-c_{fl} - c_{yfl}) \dot{z}_{fl} + k_{yfl} h_{fl} + c_{yfl} \dot{h}_{fl} + k_{yfl} \phi \cdot l - k_{yfl} \theta \cdot a \\ & + c_{yfl} \dot{\phi} \cdot l - c_{yfl} \dot{\theta} \cdot a \end{aligned}$$

$$\begin{aligned}
m_{f\bar{r}}\ddot{z}_{f\bar{r}} &= k_{f\bar{r}}z_s + c_{f\bar{r}}\dot{z}_s + (-k_{f\bar{r}} - k_{t\bar{f}\bar{r}})z_{f\bar{r}} + (-c_{f\bar{r}} - c_{t\bar{f}\bar{r}})\dot{z}_{f\bar{r}} + k_{t\bar{f}\bar{r}}h_{f\bar{r}} + c_{t\bar{f}\bar{r}}\dot{h}_{f\bar{r}} + k_{t\bar{f}\bar{r}}\phi \cdot l - k_{t\bar{f}\bar{r}}\theta \cdot a \\
&+ c_{t\bar{f}\bar{r}}\dot{\phi} \cdot l - c_{t\bar{f}\bar{r}}\dot{\theta} \cdot a \\
m_{r\bar{r}}\ddot{z}_{r\bar{r}} &= k_{r\bar{r}}z_s + c_{r\bar{r}}\dot{z}_s + (-k_{r\bar{r}} - k_{t\bar{r}\bar{r}})z_{r\bar{r}} + (-c_{r\bar{r}} - c_{t\bar{r}\bar{r}})\dot{z}_{r\bar{r}} + k_{t\bar{r}\bar{r}}h_{r\bar{r}} + c_{t\bar{r}\bar{r}}\dot{h}_{r\bar{r}} + k_{t\bar{r}\bar{r}}\phi \cdot l - k_{t\bar{r}\bar{r}}\theta \cdot a \\
&+ c_{t\bar{r}\bar{r}}\dot{\phi} \cdot l - c_{t\bar{r}\bar{r}}\dot{\theta} \cdot a \\
m_{r\bar{l}}\ddot{z}_{r\bar{l}} &= k_{r\bar{l}}z_s + c_{r\bar{l}}\dot{z}_s + (-k_{r\bar{l}} - k_{t\bar{r}\bar{l}})z_{r\bar{l}} + (-c_{r\bar{l}} - c_{t\bar{r}\bar{l}})\dot{z}_{r\bar{l}} + k_{t\bar{r}\bar{l}}h_{r\bar{l}} + c_{t\bar{r}\bar{l}}\dot{h}_{r\bar{l}} + k_{t\bar{r}\bar{l}}\phi \cdot l - k_{t\bar{r}\bar{l}}\theta \cdot a \\
&+ c_{t\bar{r}\bar{l}}\dot{\phi} \cdot l - c_{t\bar{r}\bar{l}}\dot{\theta} \cdot a
\end{aligned}$$

Rearranging all of these eight equations, the second order differential equations of this 8 DOF model can be given as (Where $X = [z_b \quad z_s \quad \theta \quad \phi \quad z_{f\bar{r}} \quad z_{r\bar{l}} \quad z_{r\bar{l}} \quad z_{r\bar{r}}]^T$):

$$M \cdot \ddot{X} + C \cdot \dot{X} + K \cdot X = F$$

In the equation, the details of each matrices are (the stiffness between sprung and unsprung mass: $k_{f\bar{l}} = k_{f\bar{r}} = k_f$, $k_{r\bar{l}} = k_{r\bar{r}} = k_r$; the damping value between sprung and unsprung mass: $c_{f\bar{l}} = c_{f\bar{r}} = c_f$, $c_{r\bar{l}} = c_{r\bar{r}} = c_r$; the stiffness of the tire: $k_{u\bar{l}} = k_{u\bar{f}\bar{r}} = k_{u\bar{r}\bar{l}} = k_{u\bar{r}\bar{r}} = k_u$; the damping value of the tire: $c_{u\bar{l}} = c_{u\bar{f}\bar{r}} = c_{u\bar{r}\bar{l}} = c_{u\bar{r}\bar{r}} = c_u$):

$$M = \begin{bmatrix}
m_b & 0 & 0 & 0 & 0 & 0 & 0 & 0 \\
0 & m_s & 0 & 0 & 0 & 0 & 0 & 0 \\
0 & 0 & J_{xx} & 0 & 0 & 0 & 0 & 0 \\
0 & 0 & 0 & J_{yy} & 0 & 0 & 0 & 0 \\
0 & 0 & 0 & 0 & m_{f\bar{r}} & 0 & 0 & 0 \\
0 & 0 & 0 & 0 & 0 & m_{r\bar{l}} & 0 & 0 \\
0 & 0 & 0 & 0 & 0 & 0 & m_{r\bar{l}} & 0 \\
0 & 0 & 0 & 0 & 0 & 0 & 0 & m_{r\bar{r}}
\end{bmatrix}$$

$$K = \begin{bmatrix}
k_b & -k_b & -k_b x_b & k_b y_b & 0 & 0 & 0 & 0 \\
-k_b & k_b + 2k_f + 2k_r & k_b x_b - 2k_f a + 2k_r b & -k_b y_b & -k_f & -k_f & -k_r & -k_r \\
-k_b x_b & k_b x_b - 2k_f a + 2k_r b & k_b x_b^2 - 2k_f a^2 + 2k_r b^2 & -k_b x_b y_b & k_f a & k_f a & -k_r b & -k_r b \\
k_b y_b & -k_b y_b & -k_b x_b y_b & k_b y_b^2 + 2k_f l^2 + 2k_r l^2 & -k_f l & k_f l & k_r l & -k_r l \\
0 & -k_f & k_f a & -k_f l & k_f + k_u & 0 & 0 & 0 \\
0 & -k_f & k_f a & k_f l & 0 & k_f + k_u & 0 & 0 \\
0 & -k_r & -k_r b & k_r l & 0 & 0 & k_r + k_u & 0 \\
0 & -k_r & -k_r b & -k_r l & 0 & 0 & 0 & k_r + k_u
\end{bmatrix}$$

$$C = \begin{bmatrix} c_b & -c_b & -c_b x_b & c_b y_b & 0 & 0 & 0 & 0 \\ -c_b & c_b + 2c_f + 2c_r & c_b x_b - 2c_f a + 2c_r b & -c_b y_b & -c_f & -c_f & -c_r & -c_r \\ -c_b x_b & c_b x_b - 2c_f a + 2c_r b & c_b x_b^2 - 2c_f a^2 + 2c_r b^2 & -c_b x_b y_b & c_f a & c_f a & -c_r b & -c_r b \\ c_b y_b & -c_b y_b & -c_b x_b y_b & c_b y_b^2 + 2c_f l^2 + 2c_r l^2 & -c_f l & c_f l & c_r l & -c_r l \\ 0 & -c_f & c_f a & -c_f l & c_f + c_u & 0 & 0 & 0 \\ 0 & -c_f & c_f a & c_f l & 0 & c_f + c_u & 0 & 0 \\ 0 & -c_r & -c_r b & c_r l & 0 & 0 & c_r + c_u & 0 \\ 0 & -c_r & -c_r b & -c_r l & 0 & 0 & 0 & c_r + c_u \end{bmatrix}$$

$$F = \begin{bmatrix} 0 & 0 & 0 & 0 & c_f \dot{h}_{fr} + k_u h_{fr} & c_f \dot{h}_{fl} + k_u h_{fl} & c_r \dot{h}_{rl} + k_u h_{rl} & c_r \dot{h}_{rr} + k_u h_{rr} \end{bmatrix}^T$$

3.1.3 Ambulance Parameters

The ambulance parameters applied to the simulations are compatible with Mercedes-Benz's Sprinter 415 CDI 7.5 m3 vehicle adapted to the ICU model, while Figure 3.1(b) illustrates the corresponding ambulance parameters. The value of all of the other parameters are summarized in the Table 3.1.

Table 3.1 Ambulance parameters

Parameters	Values	Parameters	Values
Sprung mass [kg]	2600	Front suspension stiffness [N/m]	198000
Roll inertia [kgm ²]	658	Rear suspension stiffness [N/m]	130000
Pitch inertia [kgm ²]	4174	Front suspension damping [Ns/m]	12500
Wheel centers [mm] (front & rear)	1550	Rear suspension damping [Ns/m]	12500
Front unsprung mass [kg] (both sides)	150	Tire stiffness [N/m] (front & rear)	250000
Rear unsprung mass [kg] (both sides)	100	Tire damping [Ns/m] (front & rear)	null

3.1.4 Parameter Optimization and Analysis

In this study, Matlab/Simulink software is used to simulate the dynamic behavior of this 8 DOF ambulance model. Four sinusoidal signals acting on each of the four wheels are used as inputs to this full car model and different damping and stiffness coefficients (k_b and c_b) of stretcher suspension is applied and tested in the simulation to find the optimum k_b and c_b that could minimize the vertical acceleration of the stretcher.

Since ride comfort is improved when the magnitude of vertical acceleration is reduced. So, the displacement and the acceleration of the stretcher (z_b and \ddot{z}_b) are the good indicator of comfort performance of the patients. The points chosen to calculate the acceleration, denoted as point "1" and "2" in Figure 2.1(b), will be tested respectively.

As constraints to the optimization problem, the maximum allowable jerk experienced by the patient is 18 m/s³ ($\max \ddot{z}_b = 18 \text{ m/s}^3$). In addition, if the relative displacement of the spring of the stretcher suspension is too large, the connection between stretcher and sprung mass will become rigid. Assuming the flexible length of the spring is 80 mm, the displacement of the spring during riding should be less than 80 mm ($|z_b - z + \theta \cdot x_b| \leq 0.08$, neglect the displacement caused by rolling of the sprung mass). In conclusion, the system should be limited according to the following inequality:

$$\begin{cases} 2000 \leq k_b \leq 30000 \\ 5 \leq c_b \leq 500 \\ |z_b - z + \theta \cdot x_b| \leq 0.08 \\ \ddot{z}_b \leq 18 \text{ m/s}^3 \end{cases}$$

3.2 Simulation and Results

3.2.1 Simulation of the sinusoidal road profile

In order to input the sinusoidal signals in Matlab/Simulink, we calculate the signal in time domain. Based on the ambulance speed of 30 km/h, the frequency of the signal: $w = 2\pi / (6.5 / (30 / 3.6)) = 8.0554$; the amplitude is 0.05; the bias is 0.05. The phase of the front wheels is $\varphi_f = -w \cdot (6.5 / 4 / (30 / 3.6)) = -1.5708$. The phase of the rear wheel is $\varphi_r = w \cdot (-6.5 / 4 / (30 / 3.6) + 3.25 / (30 / 3.6)) = 1.5708$. so the expression of the front and rear inputs in time domain are:

$$\begin{cases} h_f = 0.05 \sin(8.0554t - 1.5708) + 0.05 \\ h_r = 0.05 \sin(8.0554t + 1.5708) + 0.05 \end{cases}$$

The plots of the signals in time domain are shown in Figure 3.3:

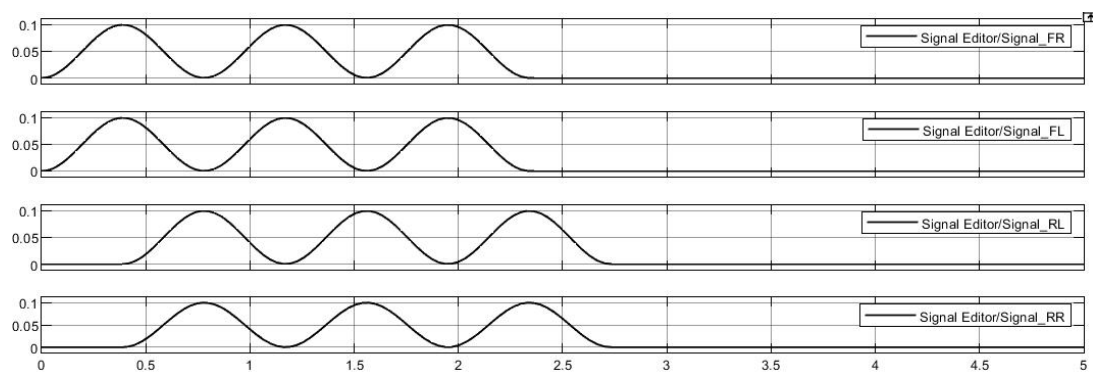


Figure 3.3 Input signals of four wheels

3.2.2 8-DOF Simulink model

In Matlab/Simulink, Based on the sets of second order differential equations in 3.2.1, the Simulink block diagram model can be built shown in Figure 3.4. The paths of the inequality described in 3.2.3 also included in this Simulink model.

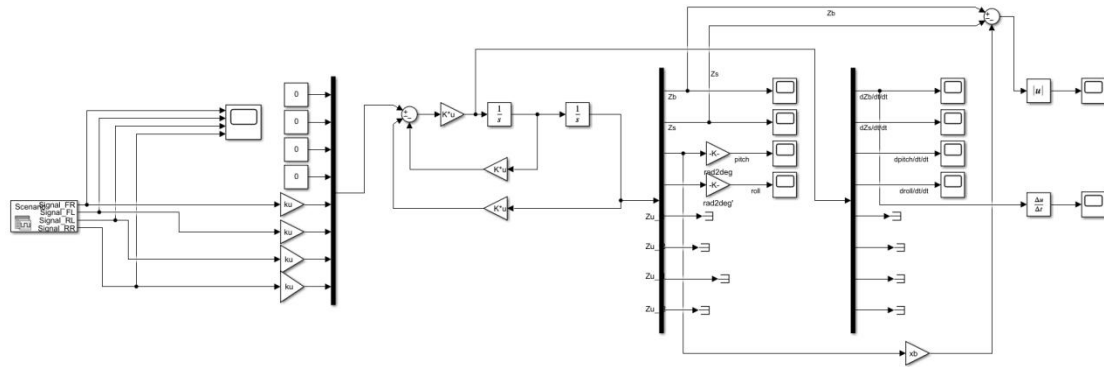


Figure 3.4 8-DOF Simulink model

3.2.3 Choosing the Optimum k_b and c_b (point “2”)

Firstly, the point “2” is analyzed. Then the same procedures are done in point “1”.

(1) Fix c_b , find the optimum k_b

The value of c_b is fixed at 300 Ns/m. Then varying k_b from 2000 to 10000. The responses of displacement and acceleration of stretcher is shown in Figure 3.5. Table 3.2 shows the comfort performance of stretcher numerically varying k_b . From the plots of the responses, we can find that the lower the k_b (softer the stretcher suspension), better the comfort responses, which matches the real case. But if the k_b is too small, the relative displacement of the spring will be larger than 80 mm, which against the requirement of the inequality in 3.2.3.

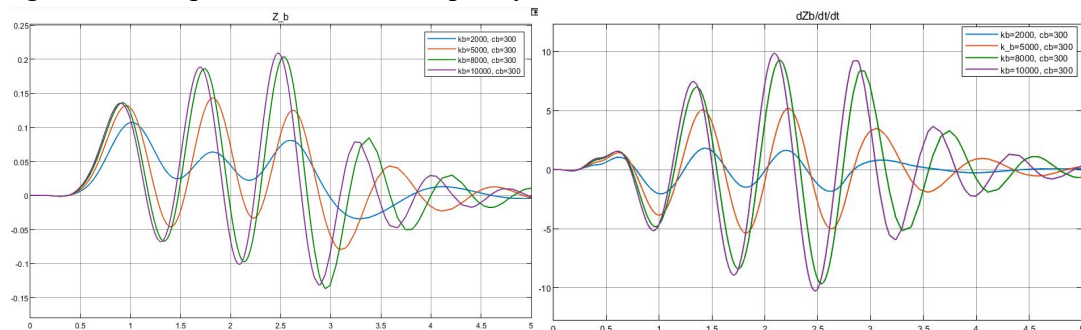


Figure 3.5 Displacement and acceleration of stretcher varying k_b of point “2”

Table 3.2 Displacement and acceleration of stretcher varying k_b of point “2”

K_b (N/m)	Vertical acceleration (m/s^2)		Vertical displacement (m)	
	Max	Min	Max	Min
2000	2.645	-2.365	0.116	-0.034
5000	5.153	-5.233	0.141	-0.075
8000	9.126	-9.837	0.200	-0.134
10000	9.935	-10.062	0.207	-0.126

(2) Fix the optimum $k_b=2000$ N/s, varying c_b .

The value of k_b is fixed at 2000 N/m. Then varying c_b from 250 to 500. The responds of displacement and acceleration of stretcher is shown in Figure 3.6. Table 3.3 shows the comfort performance of stretcher numerically varying c_b . From the plots of the responses, we can find that the best comfort performance is obtained when $c_b=350$ Ns/m.

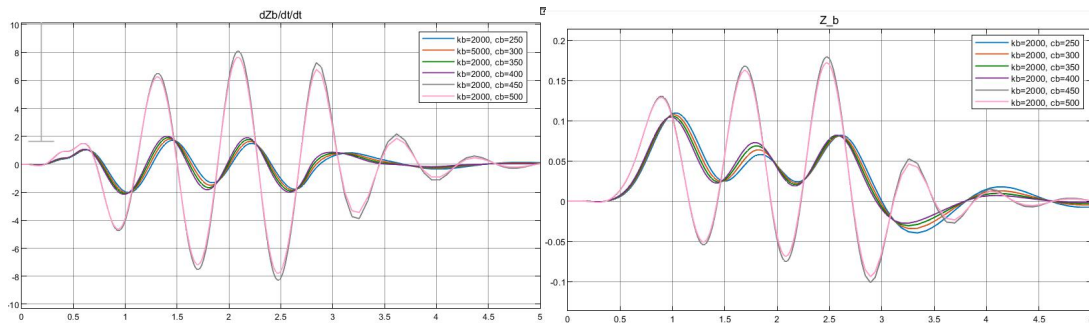


Figure 3.6 Displacement and acceleration of stretcher varying k_b of point “2”

Table 3.3 Displacement and acceleration of stretcher varying c_b of point “2”

C_b (N/m)	Vertical displacement (m)		Vertical acceleration (m/s^2)	
	Max	Min	Max	Min
250	0.117	-0.041	1.935	-1.973
300	0.114	-0.038	1.903	-1.917
350	0.109	-0.214	1.897	-1.913
400	0.109	-0.233	1.993	-2.072
450	0.174	-0.103	8.051	-8.227
500	0.168	-0.092	7.634	-7.956

Based on this optimum value of k_b and c_b , the responses of roll motion, pitch motion and vertical motion of the sprung mass are shown in Figure 3.7 to 3.14.

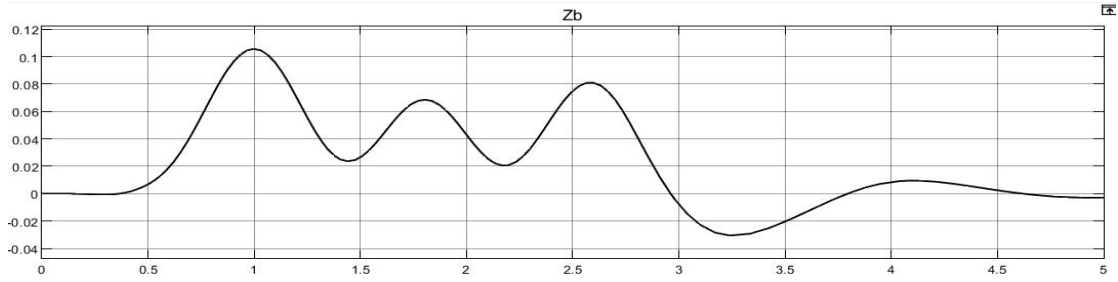


Figure 3.7 vertical displacement of stretcher of point "2"

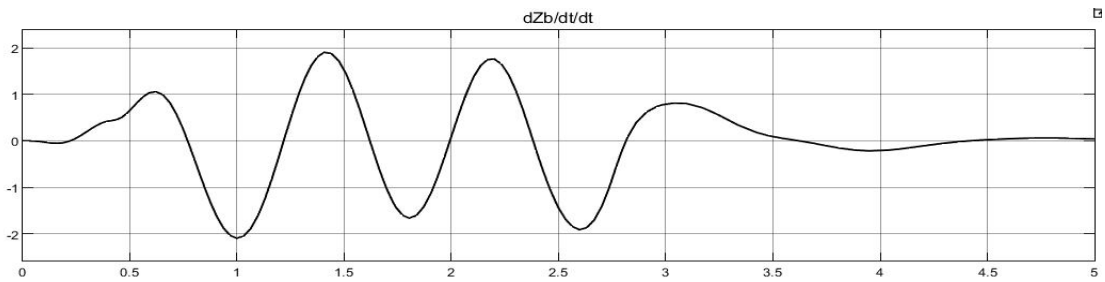


Figure 3.8 vertical acceleration of stretcher of point "2"

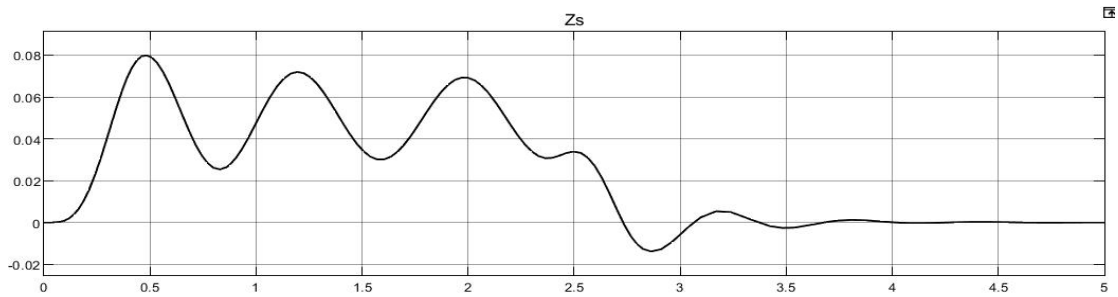


Figure 3.9 vertical displacement of sprung mass of point "2"

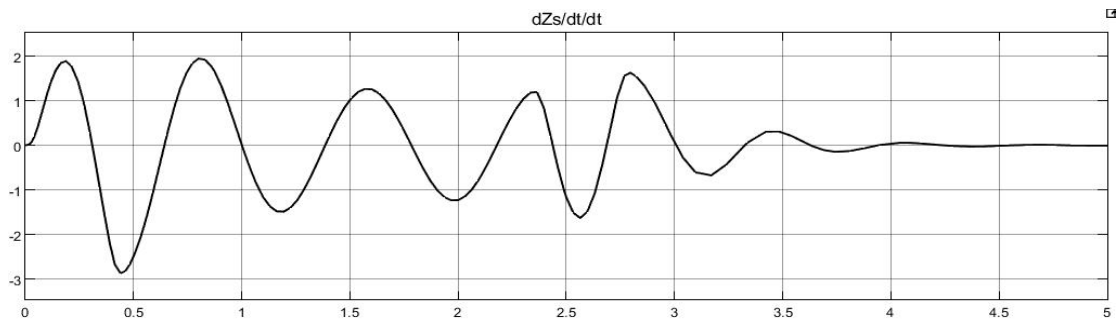


Figure 3.10 vertical acceleration of sprung mass of point "2"

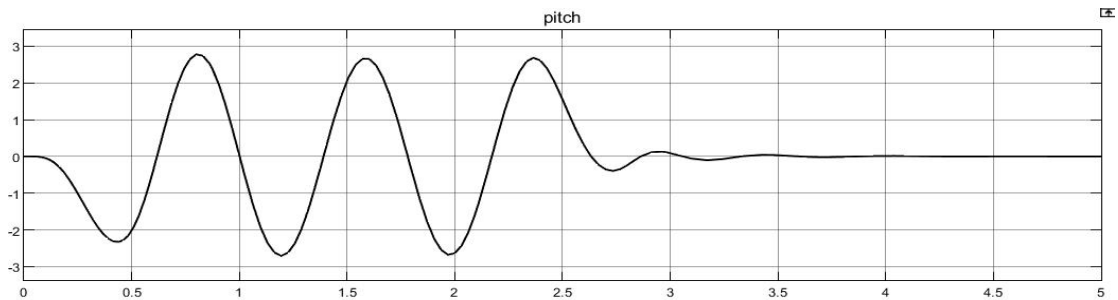


Figure 3.11 pitch of sprung mass of point "2"

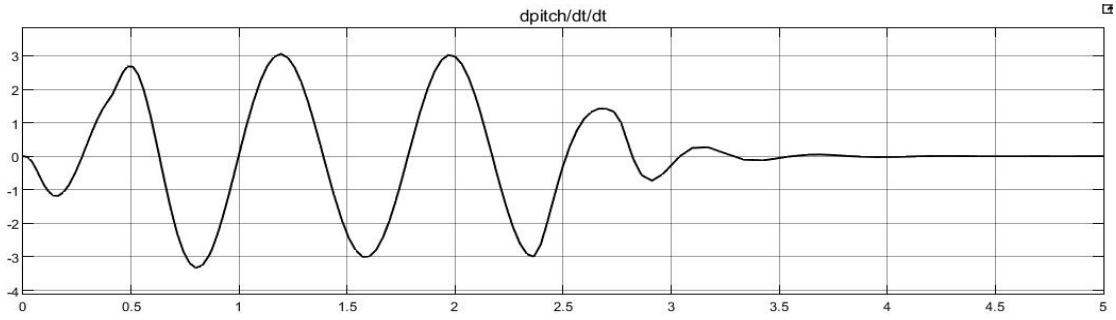


Figure 3.12 pitch acceleration of sprung mass of point “2”

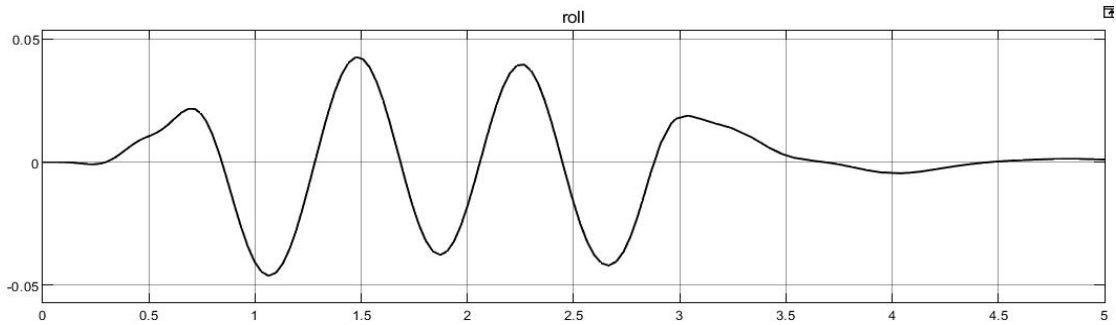


Figure 3.13 roll of sprung mass of point “2”

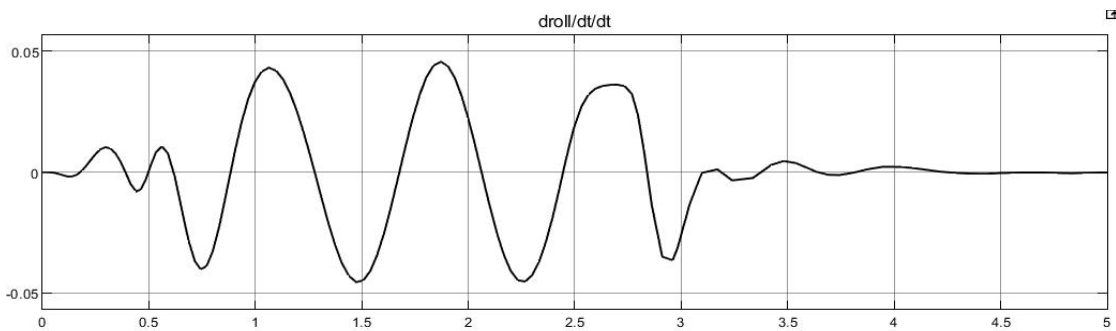


Figure 3.14 roll acceleration of sprung mass of point “2”

In addition, at this optimum value of k_b and c_b , the plots of inequality \ddot{z}_b and $|z_b - z + \theta \cdot x_b|$ are shown in Figure 3.15 and Figure 3.16. From the plots we can say that the requirements of inequality are satisfied.

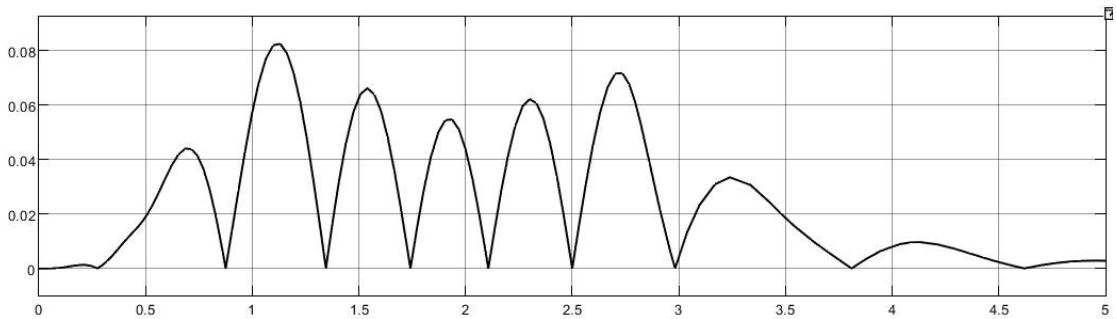


Figure 3.15 Plot of $|z_b - z + \theta \cdot x_b|$

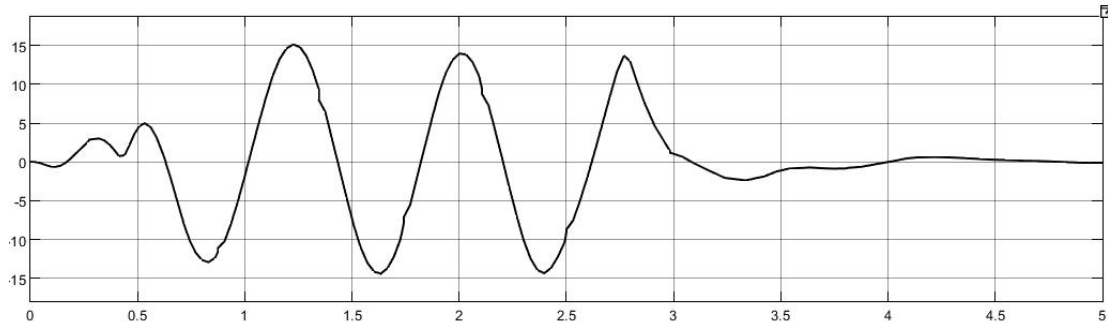


Figure 3.16 Plot of \ddot{z}_b

3.2.4 Choosing the Optimum k_b and c_b (point “1”)

In the same way of point “2”, we can simulate the vertical displacement and acceleration of point “1” varying different value of k_b and c_b . The responses of different value of k_b and c_b are shown in Figure 3.17 and 3.18. Table 3.4 and 3.5 shows the comfort performance of stretcher numerically varying k_b and c_b . From the plots, we can say that the results are exactly like what we find in point “2”. The point “1” and “2” share the same optimum k_b and c_b .

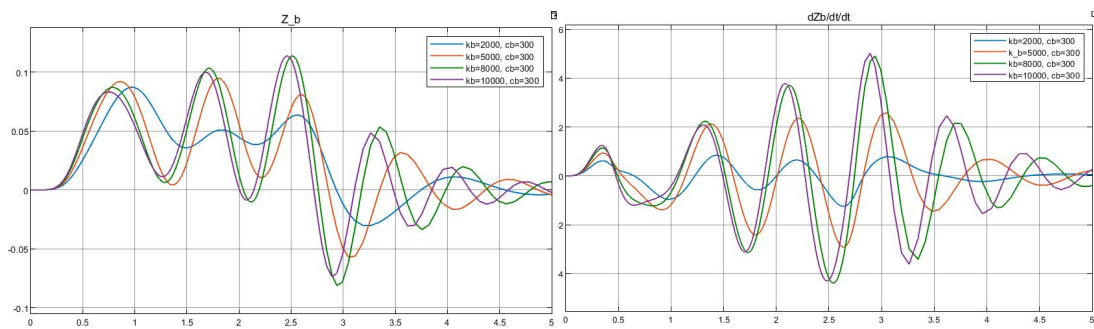


Figure 3.17 Displacement and acceleration of stretcher varying k_b of point “1”

Table 3.4 Displacement and acceleration of stretcher varying k_b of point “1”

k_b (N/m)	Vertical acceleration (m/s^2)		Vertical displacement (m)	
	Max	Min	Max	Min
2000	1.028	-1.674	0.076	-0.038
5000	2.574	-2.976	0.081	-0.068
8000	4.467	-4.453	0.127	-0.073
10000	4.253	-4.432	0.125	-0.072

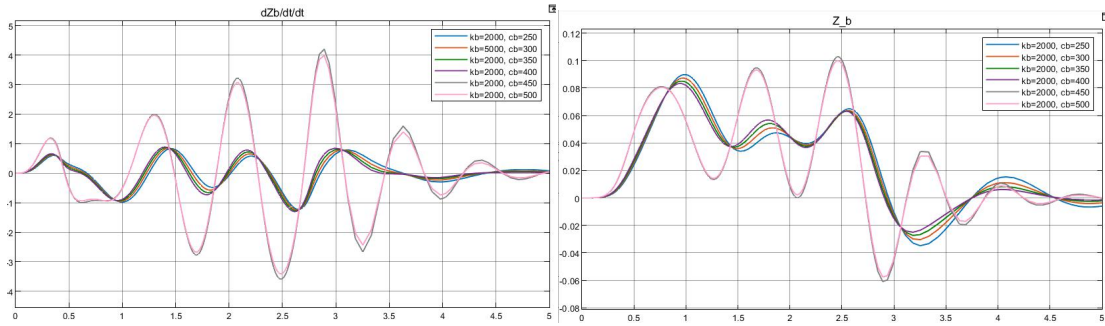


Figure 3.18 Displacement and acceleration of stretcher varying c_b of point “1”

Table 3.5 Displacement and acceleration of stretcher varying c_b of point “1”

C_b (N/m)	Vertical acceleration (m/s^2)		Vertical displacement (m)	
	Max	Min	Max	Min
250	0.717	-1.441	0.090	-0.029
300	0.613	-1.338	0.086	-0.034
350	0.502	-1.214	0.084	-0.025
400	0.563	-1.333	0.090	-0.023
450	4.074	-3.532	0.092	-0.057
500	4.148	-3.094	0.107	-0.063

Based on this optimum value of k_b and c_b , the responses of vertical motion of the stretcher are shown in Figure 3.19 to 3.20.

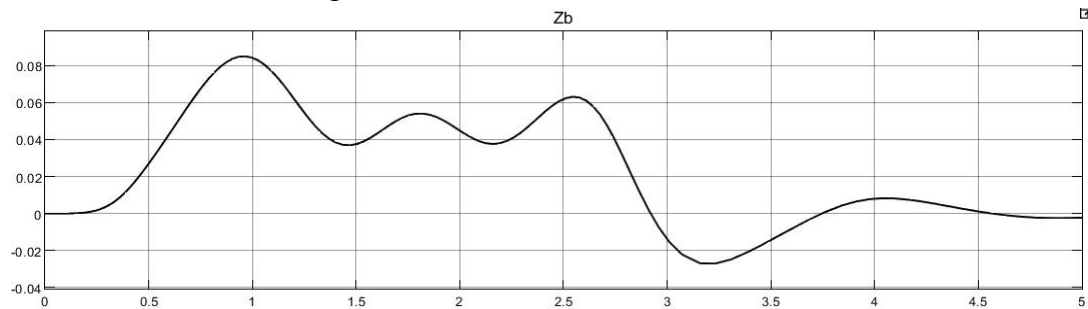


Figure 3.19 vertical displacement of stretcher of point “1”

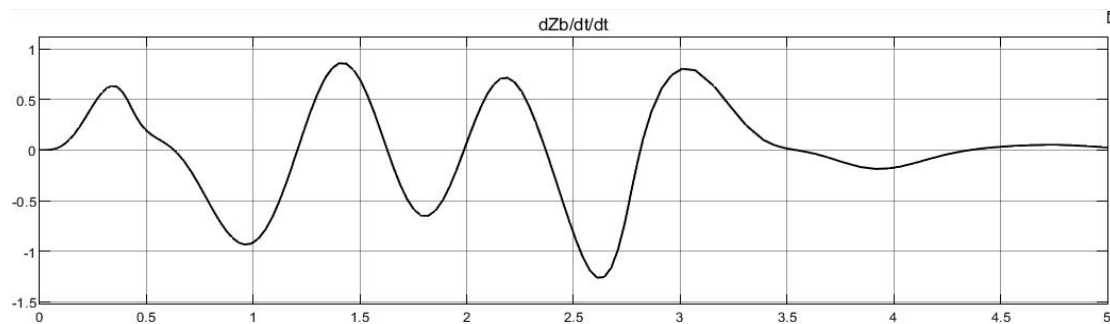


Figure 3.20 vertical acceleration of stretcher of point “1”

From the Figure 3.21 and 3.22, we can also say that this optimum value of k_b and c_b satisfy the requirement of inequality mentioned in 3.25.

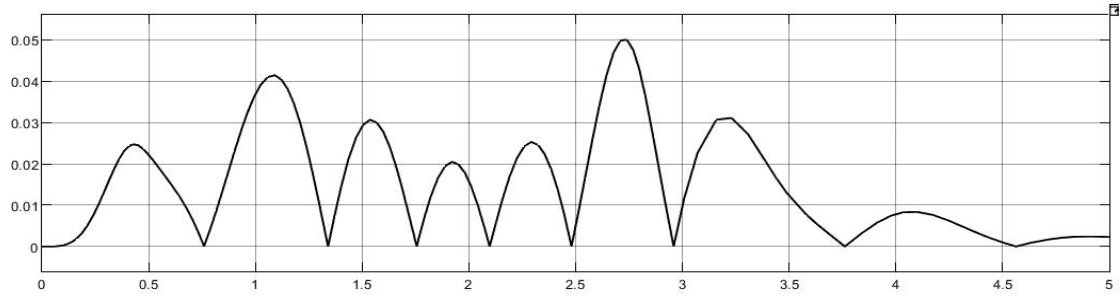


Figure 3.21 Plot of $|z_b - z + \theta \cdot x_b|$ of point "1"

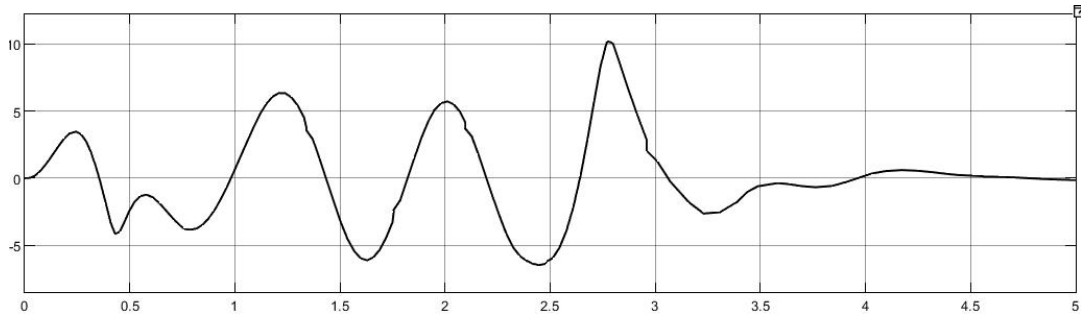


Figure 3.22 Plot of \ddot{z}_b of point "1"

3.3 Simulation of Grade C Road Profile

Uneven road is normally used to evaluate the vehicle roll stability in terms of comfort performance. According to the ISO/TC108/SC2N67 standard, random roads can be simulated in terms of the roughness coefficient $G_q(n_0)$. In this case, random road profile is simulated in equation^[4] below.

$$\dot{h}_0(t) = -2\pi f_0 \cdot h_0(t) + 2\pi n_0 \cdot \sqrt{G_q(n_0)u(t)w(t)}$$

In the equation, n_0 is a spatial reference frequency of 0.1, f_0 is a minimal boundary frequency of 0.0628 Hz, $u(t)$ is the speed in m/s, and $w(t)$ is a white noise signal. Based on this equation the block diagram of road profile on four wheels in Simulink is shown in Figure 3.23.

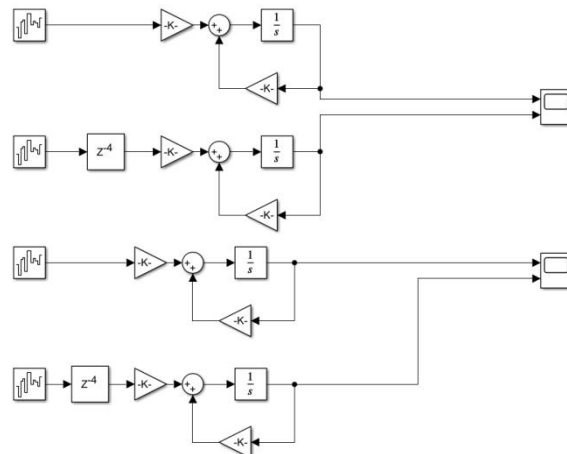


Figure 3.23 Block diagram of random road profile

The road class is ISO grade C road with a roughness coefficient of $256 \cdot 10^{-6}$. In Figure 3.24, the road excitation for each tire considering the delay between the front and rear axles, which is a significant factor for the vehicle roll motion.

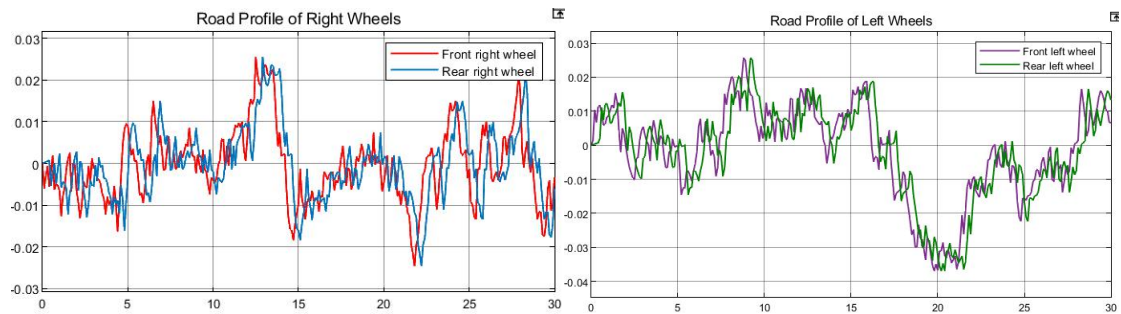


Figure 3.24 Grade C road profile of four wheels

The responses of vertical displacement and acceleration of stretcher varying different values of k_b and c_b are shown in Figure 3.25. From the plots we can verify that the optimum values of k_b and c_b ($k_b=2000$ N/m, $c_b=350$ Ns/m) also valid in random road profile.

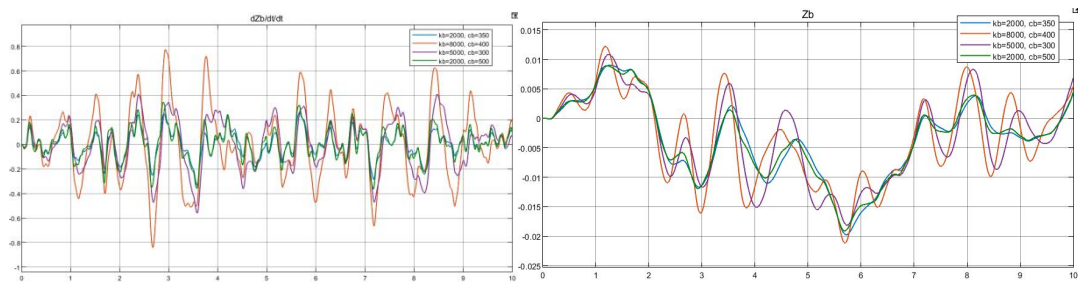


Figure 3.25 vertical displacement and acceleration of stretcher on random road profile

Chapter 4

Confirm Optimal k_b and c_b

4.1 Influence of k_b and c_b to Comfort of the Patient

From the previous study we can see that difference values of k_b and c_b have a great influence on vertical displacement and acceleration of the patient on the stretcher. We can make a plot of a indicator of comfort performance of patient varying k_b and c_b , showing the influence of k_b and c_b on \ddot{z}_b more clearly and find the optimum value of k_b and c_b more accurately.

4.1.1 RMS value of the signal

One good indicator of the comfort performance of the patients is the plot of \ddot{z}_b . But it is more convenient to use just one value to represent the comfort of the patients in a defined condition. The mean value of \ddot{z}_b is equal to zero. The mean square value of \ddot{z}_b can be a good indicator, but in this case the unit of the indicator will be different from \ddot{z}_b . To not change the unit, the RMS (Root Mean Square) value of \ddot{z}_b can be used as the indicator of comfort performance of the patient.

The RMS value of a signal $f(t)$ can be expressed as the equation below:

$$RMS = \sqrt{\frac{1}{T} \int_{-T}^T f(t)^2 dt}$$

Where $f(t)$ is the function of the signal in time domain. T is the total time of the signal. For example if we have a plot of \ddot{z}_b like in figure 4.1, the RMS value of the signal can be seen as the root of the area between the signal and the horizontal axis. So, lower the RMS of \ddot{z}_b , better the comfort performance of the patient.

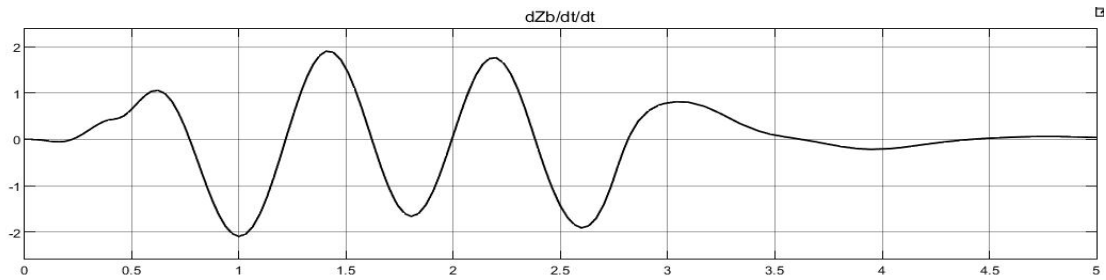


Figure 4.1 Plot of $f(t)$

Based on the grade C random road as input, fixing the k_b and c_b value, using the ambulance model we obtained before, we can plot \ddot{z}_b in time domain in Matlab/Simulink. Then using the block “To workplace” in Simulink, all of the data in this plot can be output to Matlab workplace. In this way, using some Matlab code the RMS value of these data can be calculated. For example, if $k_b=2000$, $c_b=350$, the RMS value of \ddot{z}_b is 4.3963.

4.1.2 RMS value of \ddot{z}_b varying k_b

To analyse the influence of k_b on the RMS value of \ddot{z}_b , we fix the damping value $c_b=200$, the velocity of the ambulance $V=30$ km/h and varying the k_b from 2000 to 10000 at the distance of 250. With each value of k_b corresponding to one value of RMS, all of the value of RMS of \ddot{z}_b can be plotted. As a comparison, the RMS of \ddot{z}_s can also be plotted. The results shows in Figure 4.2.

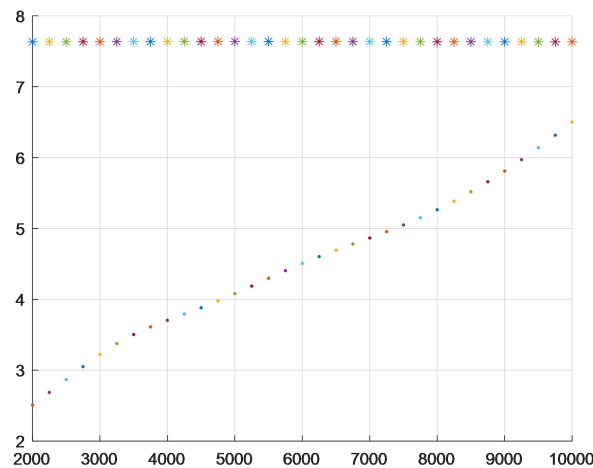


Figure 4.2 RMS of \ddot{z}_b and \ddot{z}_s varying k_b

In this figure, “.” represent the RMS values of \ddot{z}_b ; “*” represent the RMS values of \ddot{z}_s . From the Figure, the relation between RMS and k_b is clear: lower the k_b , lower the RMS of \ddot{z}_b , better the comfort of the patients. In addition, the RMS of \ddot{z}_s is much higher than the RMS value of \ddot{z}_b , meaning that the comfort performance of the patients is much better than the comfort of sprung mass (ex. the driver). RMS values

of \ddot{z}_s can also represent the comfort performance in the case that the connection between the stretcher and the sprung mass is rigid. In this case, we can find that the use of stretcher suspension greatly improve the comfort of the patients. Furthermore, it is clear that the RMS of \ddot{z}_s are almost not influenced by the changing of k_b .

4.1.3 RMS value of \ddot{z}_b varying c_b

In the same way, we fix the k_b at its optimum value 2000. Then, varying the value of c_b from 50 to 1000, at the distance of 25. With each c_b value corresponding to one RMS value of \ddot{z}_b and one of the \ddot{z}_s . The results shown in Figure 4.3.

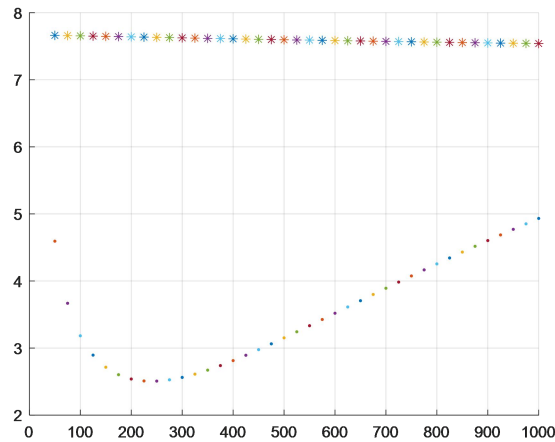


Figure 4.3 RMS of \ddot{z}_b and \ddot{z}_s varying c_b

In this figure, “.” represent the RMS values of \ddot{z}_b ; “*” represent the RMS values of \ddot{z}_s . From the Figure, the relation between RMS and c_b is not like in varying k_b . In this case, there is a c_b that corresponding to the minimum value of RMS of \ddot{z}_b , which is c_b equal to 250. In addition, the RMS value of \ddot{z}_s approximately not influenced by different values of c_b .

4.1.4 Responses of the system based on optimum value of k_b and c_b

In this way, we obtain the accurate optimum values of k_b and c_b corresponding to the best comfort performance of the patients when ambulance is riding on the random road. The optimum values are: $k_b=2000$ N/m, $c_b=250$ Ns/m.

Based on this optimum value of k_b and c_b , the responses of roll motion, pitch motion and vertical motion of the sprung mass and vertical motion of stretcher are shown in Figure 4.4 to 4.7.

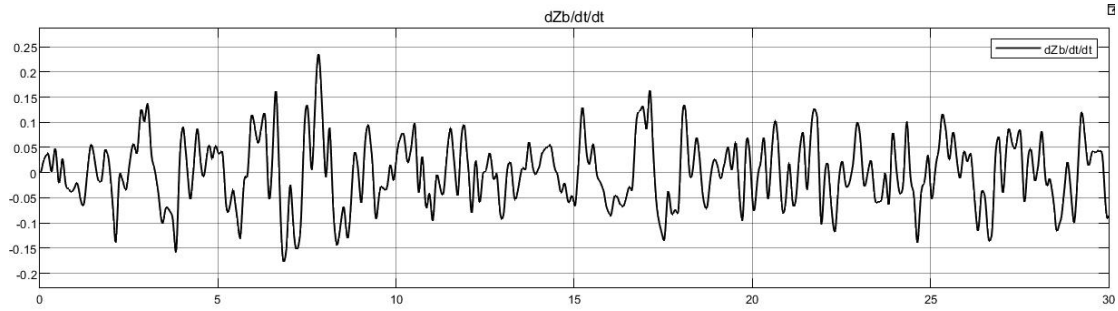


Figure 4.4 Vertical acceleration of the stretcher

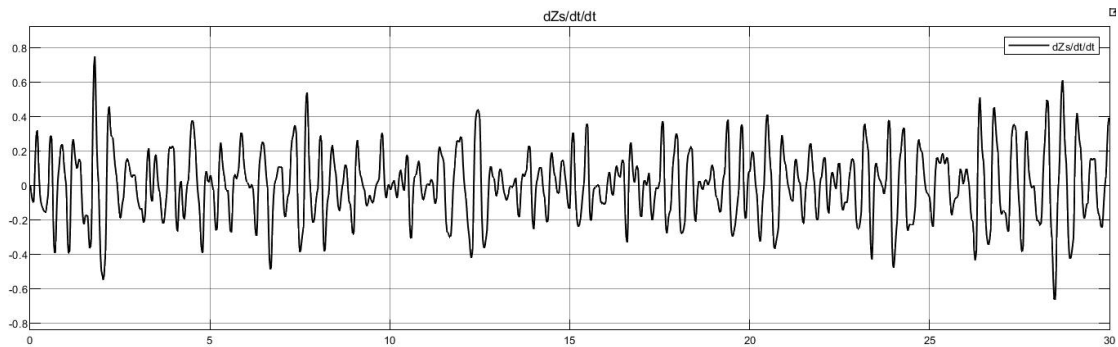


Figure 4.5 Vertical acceleration of the sprung mass

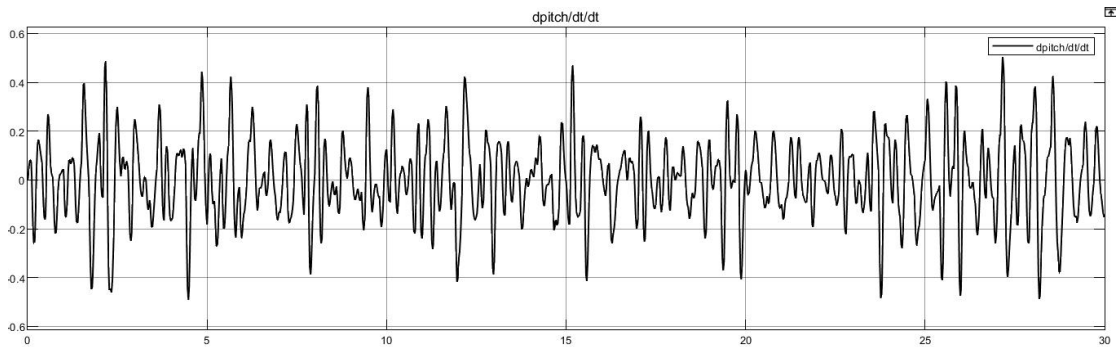


Figure 4.6 Acceleration of pitch motion of the sprung mass

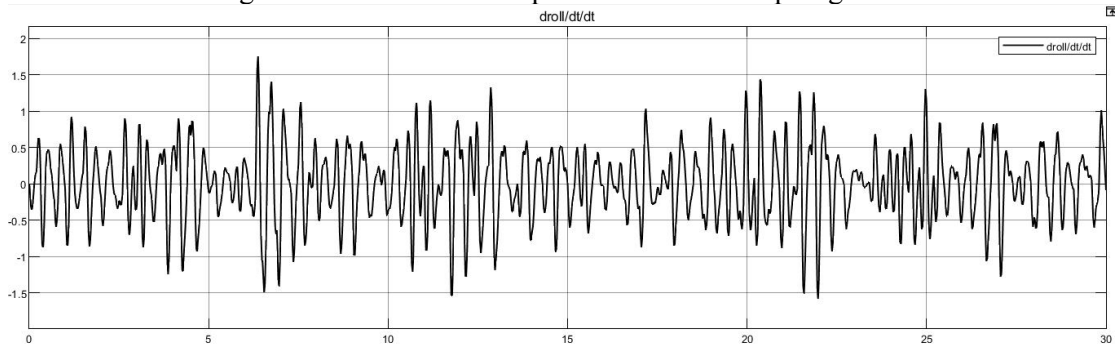


Figure 4.7 Acceleration of roll motion of the sprung mass

4.2 Influence of Speed of Ambulance to the Results

In real case, when ambulance is riding on the road, the speed of the ambulance is certainly not constant, and often much higher than 30 km/h, and the comfort performance of the patients is certainly not the same as the results obtained in 30

km/h. In this case, the influence of different speed on choosing optimum value of cb and on comfort performance of the patients and will be analyzed.

4.2.1 Influence of different speed on comfort of the patients

In this chapter, kb and cb will be fixed ($kb=2000$, $cb=250$) and the RMS of \ddot{z}_b is still be used as the indicator of the comfort of the patients. To analyse the influence of different speeds on RMS value of \ddot{z}_b , instead of varying kb and cb , we vary the speed of the ambulance from 10 km/h to 120 km/h, and output all the values of RMS corresponding to each values of the speed. The results is shown in Figure 4.8.

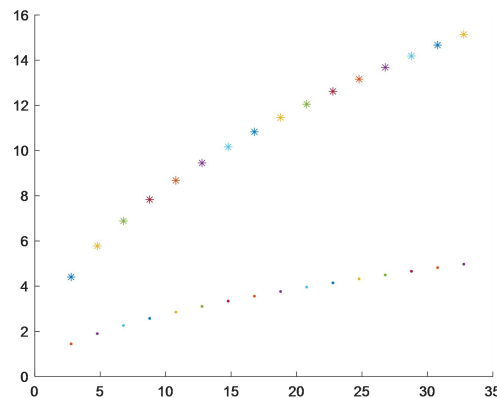


Figure 4.8 RMS of \ddot{z}_b and \ddot{z}_s from 10km/h to 120 km/h

In this figure, “.” represent the RMS values of \ddot{z}_b ; “*” represent the RMS values of \ddot{z}_s . The figure tells us that higher the speed, higher the values of the RMS, worse the comfort performance of the patients. In addition, comparing to the comfort of the patients, the comfort of the sprung mass is much more sensitive to the change of the speed.

To further verify the results, we build the model in Matlab Simulink with a defined profile of the speed as input, and the time domain responses of vertical acceleration of patients and sprung mass, acceleration of pitch motion and roll motion of sprung mass as output. The Simulink diagram is shown in Figure 4.9.

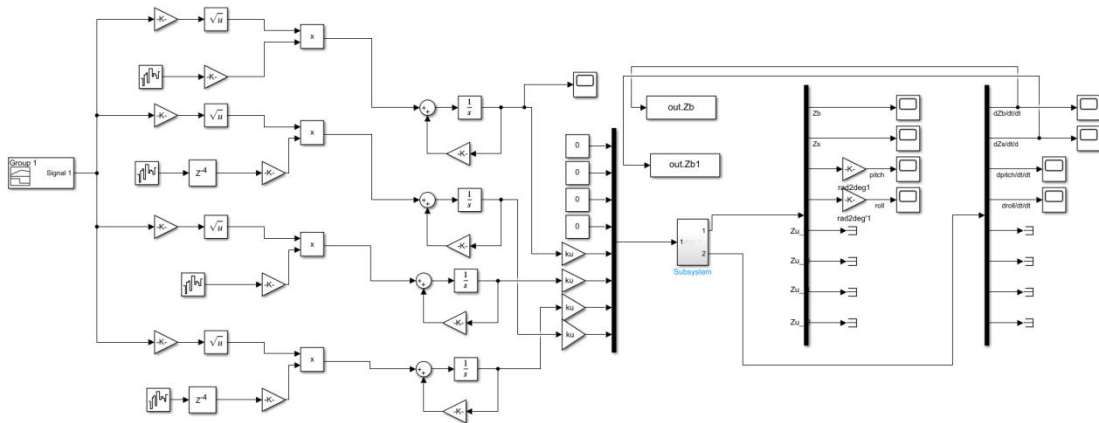


Figure 4.9 Random road profile Simulink diagram as input of a defined speed profile

Taking front right wheel as an example, the plot of defined speed profile is shown in Figure 4.10.

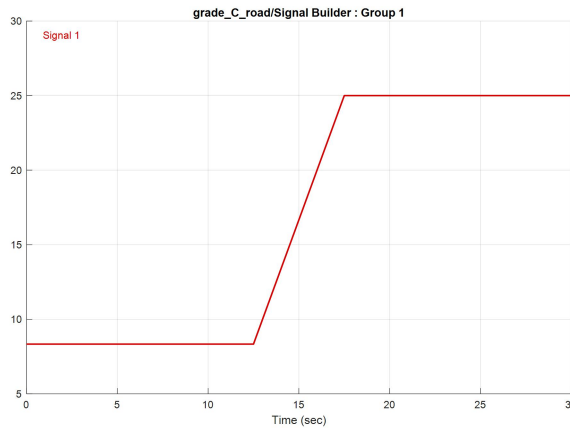


Figure 4.10 Defined profile of the speed

The ambulance is riding at constant speed of 30 km/h for 12.5 seconds and accelerate to 90 km/h by 5 seconds and keep the speed at 90 km/h for 12.5 second (30 seconds in total). The outputs is shown from Figure 4.11 to 4.14.

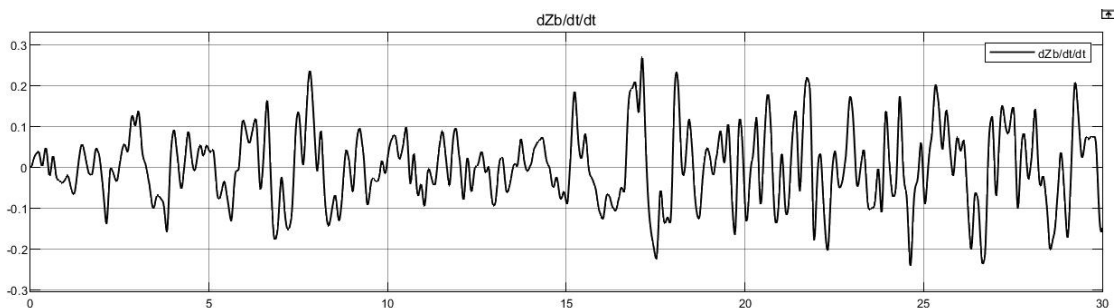


Figure 4.11 Output of \ddot{z}_b

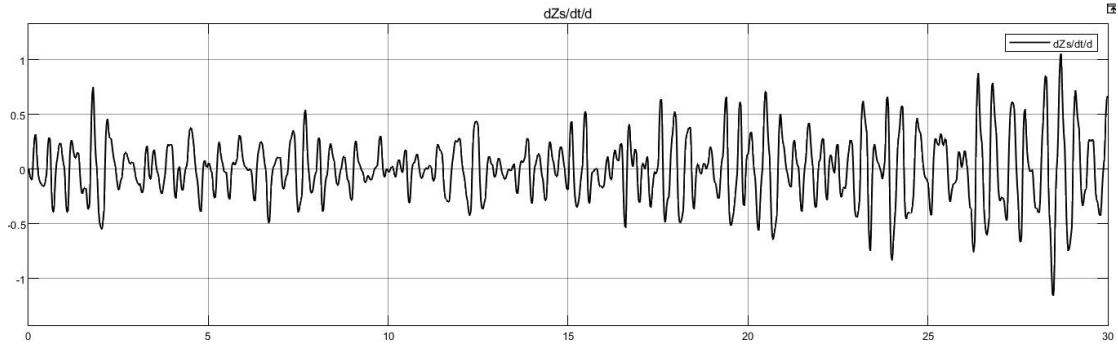


Figure 4.12 Output of \ddot{z}_s

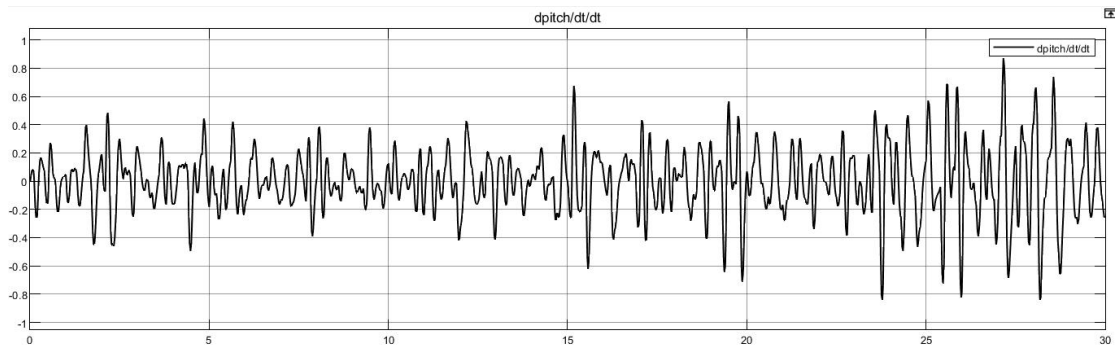


Figure 4.13 Output of acceleration of pitch motion of sprung mass

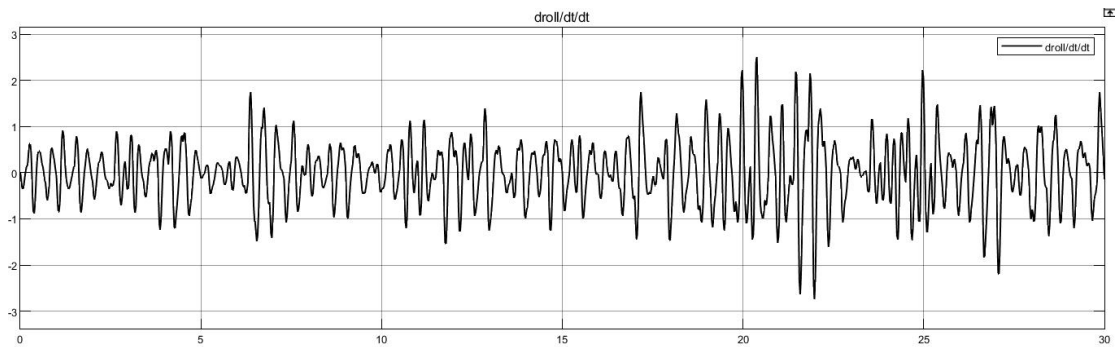


Figure 4.14 Output of acceleration of roll motion of sprung mass

In those four plots, the amplitude of first 12.5 seconds of the responses is lower than last 12.5 seconds of the responses.

4.2.2 Influence of different speed on choosing optimum and c_b

In this chapter, four different values of the speed is tested and at the same time varying c_b . The values of RMS of \ddot{z}_b in each different values of speed and c_b is shown in Figure 4.15.

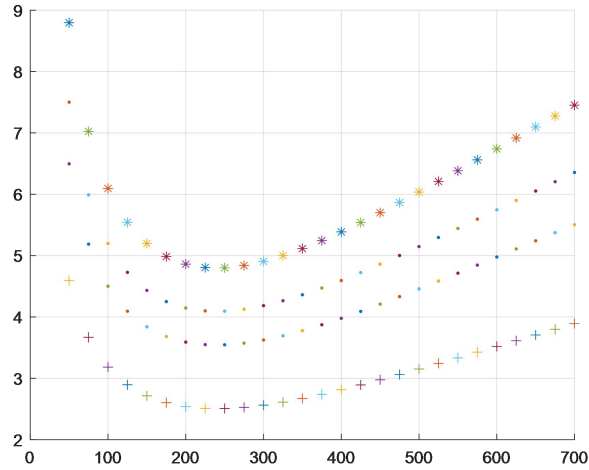


Figure 4.15 RMS of \ddot{z}_b varying speed and c_b

In this figure there are approximately four curves, corresponding to four different speeds: $V=30$ km/h, $V=45$ km/h, $V=60$ km/h, $V=90$ km/h. We can find that no matter what the speed is, the lowest value of RMS all at the same value of $c_b=250$. Changing the speed does not influence the optimum value of c_b .

4.3 Comparison Between Sinusoidal and Random Road Profile

In this chapter, the road excitation is changed to see if the optimum value of c_b is affected or not. The results of RMS values of \ddot{z}_b varying c_b from 50 to 1000, at the distance of 20, is shown in Figure 4.16. The results are obtained from sinusoidal and random road profile respectively.

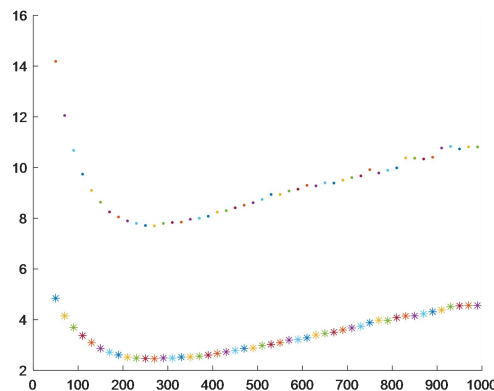


Figure 4.16 RMS of \ddot{z}_b varying c_b in sinusoidal and random road profile

From the figure, it is clear that different road profile does not influence the optimum value of c_b . So the same optimum value of c_b can be applied to the cases of different road profiles.

Chapter 5

HIS Ambulance Model

Following ^[9], in this chapter, the Hydraulic Interconnected Suspension (HIS) is added to the conventional suspension of the ambulance to further improve the comfort performance of the ambulance.

Particularly, there is a trade off among ride comfort, roll, and pitch dynamics. For example, the optimal roll-resistant performance of the vehicle is usually accompanied with excessive pitch-resistant moment, which would decrease the ride comfort of the vehicle. On the other hand, increasing the ride comfort would reduce the roll- and pitch-resistant performance.

In this study, the mathematical model of HIS suspension is built and coupled together with 8 DOF ambulance model forming a new dynamic model. Then based on this new model, the RMS values of acceleration of Z_b , Z_s , pitch motion and roll motion of the sprung mass are used as the indicators of the comfort performance of the ambulance. Then, the key parameters of the HIS suspension are varied in order to find their optimum value corresponding to the best trade off between each indicators and achieve an overall optimal performance of the ambulance. In the end, based on these optimum parameters, the comfort performance of ambulance with HIS suspension is compared with conventional suspension to verify our conclusion.

5.1 Working Principle of HIS Suspension

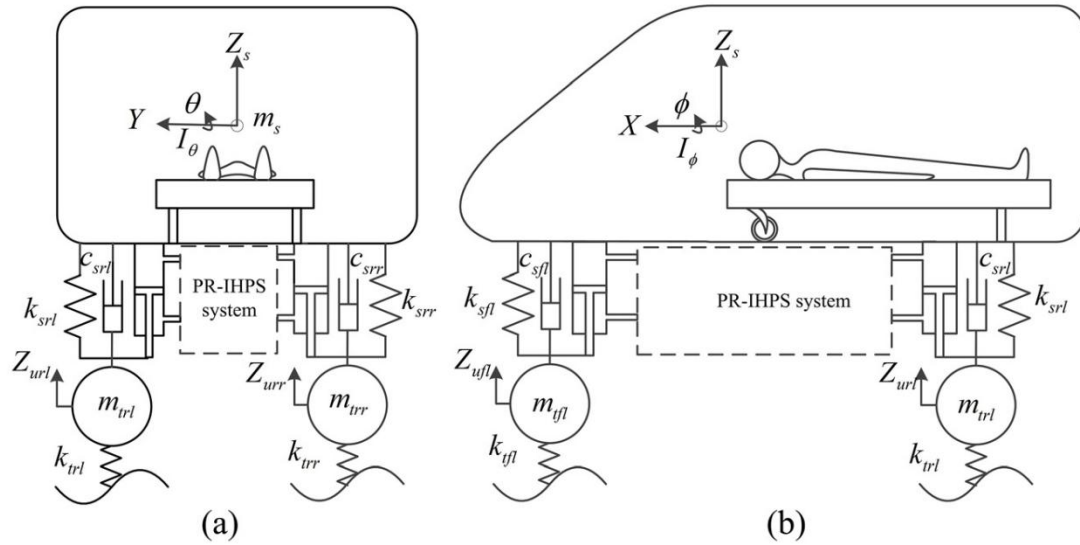


Figure 5.1 8 DOF ambulance with HIS suspension

The scheme of HIS subsystem is shown in Figure 5.2. The entire HIS system consists of four circuits connecting the different chambers. The components of each circuit include one nitrogen-filled diaphragm accumulator, one three-way junction, three damper valves and a few fluid pipelines.

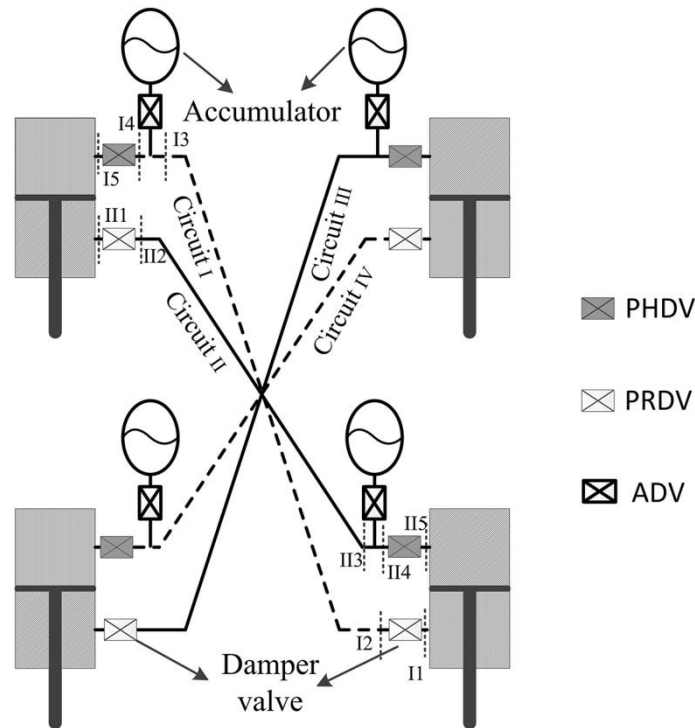


Figure 5.2 Scheme of HIS subsystem

When the ambulance turns left, positive roll motion between the sprung mass and unsprung masses occurs, and two left double-acting hydraulic cylinders are extended while right two double-acting hydraulic cylinders are compressed. At this point, hydraulic fluid in circuits I and III are lowly pressurized while ones in circuits II and

IV are highly pressurized, which collectively provide a roll restoring moment to prevent the roll motion of sprung mass relative unsprung mass. There is a similar function when the ambulance turns right.

When the ambulance brakes, positive pitch motion will occur, which means the two front double-acting hydraulic cylinders are to be compressed while the rear ones extended. As a consequence, the HIS system provides a pitch restoring moment. With respect to bounce and warp motion modes, compression and extension of double-acting hydraulic cylinders lead to hydraulic fluid in circuits flows into extension chamber from compression chamber, which results in that the fluid pressure is almost unchanged. Therefore, the HIS system only provides additional damping forces but additional stiffness is not offered.

5.2 Mathematical Model of HIS Subsystem

To coupling the HIS subsystem with the 8 DOF ambulance model, the hydraulic forces are regarded as external force:

$$M \cdot \ddot{x} + C \cdot \dot{x} + K \cdot x = F_h + F_w$$

In this equation, $x = [z_b \ z_s \ \theta \ \phi \ z_{fr} \ z_{fl} \ z_{rl} \ z_{rr}]^T$, matrices M, C, K are defined in ambulance model part. $F_w = [0 \ 0 \ 0 \ 0 \ k_u h_{fr} \ k_u h_{fl} \ k_u h_{rl} \ k_u h_{rr}]^T$ is the road excitation. F_h is the hydraulic forces. It can be expressed as $F_h = D_{p(8 \times 8)} \cdot P_{(8 \times 1)}$. The pressure matrix $P = [P_{flT} \ P_{flB} \ P_{frT} \ P_{frB} \ P_{rlT} \ P_{rlB} \ P_{rrT} \ P_{rrB}]^T$ and the area coefficient matrix D_p can be written as:

$$D_{p(8 \times 8)} = \begin{bmatrix} 0 & 0 & 0 & 0 & 0 & 0 & 0 & 0 \\ S_{flT} & -S_{flB} & S_{frT} & -S_{frB} & S_{rlT} & -S_{rlB} & S_{rrT} & -S_{rrB} \\ -aS_{flT} & aS_{flB} & -aS_{frT} & aS_{frB} & bS_{rlT} & -bS_{rlB} & bS_{rrT} & -bS_{rrB} \\ lS_{flT} & -lS_{flB} & -lS_{frT} & lS_{frB} & lS_{rlT} & -lS_{rlB} & -lS_{rrT} & lS_{rrB} \\ -S_{flT} & S_{flB} & 0 & 0 & 0 & 0 & 0 & 0 \\ 0 & 0 & -S_{frT} & S_{frB} & 0 & 0 & 0 & 0 \\ 0 & 0 & 0 & 0 & -S_{frB} & S_{rlB} & 0 & 0 \\ 0 & 0 & 0 & 0 & 0 & 0 & -S_{rrT} & -S_{rrB} \end{bmatrix}$$

Since each fluid circuit is made up of one nitrogen-filled diaphragm accumulator, one three-way junction, three damper valves, and a few fluid pipelines components, as illustrated in Figure 5.2. Thus, using the fluid element lumped-parameter method, the mathematical relationship of flow rate and pressure in the circuit between upside and downside can be determined by a sequence of multiplications of the involved fluid component impedance matrices:

$$\begin{bmatrix} P_D^k \\ Q_D^k \end{bmatrix} = T^v \times T^t \times T^p \times T^v \begin{bmatrix} P_U^k \\ Q_U^k \end{bmatrix} = \begin{bmatrix} T_{11}^k & T_{12}^k \\ T_{21}^k & T_{22}^k \end{bmatrix} \begin{bmatrix} P_U^k \\ Q_U^k \end{bmatrix} (*)$$

In this equation, “D” represent the downside of the flow, while “U” represent the upside of the flow. “v, t, p” represent each component of the system (“v” for damper valves and , “p” for pipelines and “t” for accumulator and ADV valve and three way conjunction). Matrices T is the fluid component impedance matrices. “k” represent the four circuits respectively (k=c1,c2,c3,c4 for each of the four circuits).

(1) Pipelines component impedance matrix T_p

The hydrodynamic equations of pipeline fluid element can be expressed as:

$$\begin{cases} P_U - P_D = R_p Q + I_p \dot{Q} \\ Q_U - Q_D = C_p \dot{P} \end{cases} \quad \begin{cases} P = (P_U + P_D) / 2 \\ Q = (Q_U + Q_D) / 2 \end{cases}$$

Combining these two sets of equations, then do Laplace transform with zero initial condition. The relationship of flow and pressure between upside and downside in the pipelines components can be described by the impedance matrix T_p :

$$\begin{bmatrix} P_D \\ Q_D \end{bmatrix} = \begin{bmatrix} \frac{I_p s + R_p + 4s^{-1} / C_p}{-I_p s - R_p + 4s^{-1} / C_p} & -\frac{4(I_p s + R_p)s^{-1} / C_p}{-I_p s - R_p + 4s^{-1} / C_p} \\ \frac{4}{-I_p s - R_p + 4s^{-1} / C_p} & \frac{I_p s + R_p + 4s^{-1} / C_p}{-I_p s - R_p + 4s^{-1} / C_p} \end{bmatrix} \begin{bmatrix} P_U \\ Q_U \end{bmatrix} = T^p \begin{bmatrix} P_U \\ Q_U \end{bmatrix}$$

(2) Damper valve component impedance matrix T_v

The hydrodynamic equation of this component can be written as (Z_H is the pressure loss coefficients of damper valve):

$$\begin{bmatrix} P_D \\ Q_D \end{bmatrix} = \begin{bmatrix} 1 & -Z_H \\ 0 & 1 \end{bmatrix} \begin{bmatrix} P_U \\ Q_U \end{bmatrix} = T^v \begin{bmatrix} P_U \\ Q_U \end{bmatrix}$$

(3) Accumulator, ADV valve and conjunction component impedance matrix T_v

The hydrodynamic equation of upside and downside of these combined component can be written as (Z_A is the pressure loss coefficients of ADV valve, C_a is the capacity of gas-filled diaphragm accumulator):

$$\begin{bmatrix} P_D \\ Q_D \end{bmatrix} = \begin{bmatrix} 1 & 0 \\ \frac{1}{-1/(sC_a) - Z_A} & 1 \end{bmatrix} \begin{bmatrix} P_U \\ Q_U \end{bmatrix} = T^t \begin{bmatrix} P_U \\ Q_U \end{bmatrix}$$

Substituting all of those three sets of hydrodynamic equations into equation (*) and rearrange the equation to describe the relationship between P and Q instead of upside

and downside, and expanding the expressions to all four circuits. The relationship between P and Q can be written as:

$$P = T(s) \cdot Q$$

In this equation, $Q = [Q_{fT} \quad Q_{fB} \quad Q_{frT} \quad Q_{frB} \quad Q_{rT} \quad Q_{rB} \quad Q_{rrT} \quad Q_{rrB}]^T$ is the flow rate in different chambers. T(s) is the total impedance matrix of the whole HIS subsystem. T(s) can be expressed as:

$$T(s) = \begin{bmatrix} -\frac{T_{22}^{c1}}{T_{21}^{c1}} & 0 & 0 & 0 & 0 & 0 & 0 & \frac{1}{T_{21}^{c1}} \\ 0 & \frac{T_{11}^{c2}}{T_{21}^{c2}} & 0 & 0 & 0 & 0 & \frac{T_{12}^{c2}T_{21}^{c2} - T_{11}^{c2}T_{22}^{c2}}{T_{21}^{c2}} & 0 \\ 0 & 0 & -\frac{T_{22}^{c3}}{T_{21}^{c3}} & 0 & 0 & \frac{1}{T_{21}^{c3}} & 0 & 0 \\ 0 & 0 & 0 & \frac{T_{11}^{c4}}{T_{21}^{c4}} & \frac{T_{12}^{c4}T_{21}^{c4} - T_{11}^{c4}T_{22}^{c4}}{T_{21}^{c4}} & 0 & 0 & 0 \\ 0 & 0 & 0 & \frac{1}{T_{21}^{c4}} & -\frac{T_{22}^{c4}}{T_{21}^{c4}} & 0 & 0 & 0 \\ 0 & 0 & \frac{T_{12}^{c3}T_{21}^{c3} - T_{11}^{c3}T_{22}^{c3}}{T_{21}^{c3}} & 0 & 0 & \frac{T_{11}^{c3}}{T_{21}^{c3}} & 0 & 0 \\ 0 & \frac{1}{T_{21}^{c2}} & 0 & 0 & 0 & 0 & -\frac{T_{22}^{c2}}{T_{21}^{c2}} & 0 \\ \frac{T_{12}^{c1}T_{21}^{c1} - T_{11}^{c1}T_{22}^{c1}}{T_{21}^{c1}} & 0 & 0 & 0 & 0 & 0 & 0 & \frac{T_{11}^{c1}}{T_{21}^{c1}} \end{bmatrix}$$

In addition, the flow rate Q(t) in different chamber can be described by cross-sectional areas of the chambers multiplies the speed of changing of the chamber volume. In this case, Q(t) can be expressed as:

$$Q(t) = D_m \cdot \dot{x}(t)$$

In this equation, D_m describe the cross-sectional areas responding to different speeds of all 8 degrees of freedoms.

$$D_m = \begin{bmatrix} 0 & -S_{frT} & aS_{frT} & -lS_{frT} & S_{frT} & 0 & 0 & 0 \\ 0 & -S_{frB} & aS_{frB} & -lS_{frB} & S_{frB} & 0 & 0 & 0 \\ 0 & -S_{fT} & aS_{fT} & lS_{fT} & 0 & S_{fT} & 0 & 0 \\ 0 & -S_{fB} & aS_{fB} & lS_{fB} & 0 & S_{fB} & 0 & 0 \\ 0 & -S_{rT} & -bS_{rT} & -lS_{rT} & 0 & 0 & S_{rT} & 0 \\ 0 & -S_{rB} & -bS_{rB} & -lS_{rB} & 0 & 0 & S_{rB} & 0 \\ 0 & -S_{rrT} & -bS_{rrT} & lS_{rrT} & 0 & 0 & 0 & S_{rrT} \\ 0 & -S_{rrB} & -bS_{rrB} & lS_{rrB} & 0 & 0 & 0 & S_{rrB} \end{bmatrix}$$

To sum up, the external forces F_h representing the HIS subsystem can be expressed by the following equations:

$$F_h = D_p \cdot T(s) \cdot D_m \cdot \dot{x}$$

5.3 Integration of Ambulance Model and HIS Suspension Model

After obtaining the HIS suspension mathematical model, the integrated model of HIS suspension and ambulance can be written as:

$$M \cdot \ddot{x} + C \cdot \dot{x} + K \cdot x = D_p \cdot T(s) \cdot D_m \cdot \dot{x} + F_w$$

To further integrate these two models, the external forces F_h can be further arranged to the differential equation forms like this:

$$D_p \cdot T(s) \cdot D_m \cdot \dot{x} = C_{HIS} \cdot \dot{x} + K_{HIS} \cdot x$$

In this case, the combined mathematical model can be written as:

$$M \cdot \ddot{x} + (C - C_{HIS}) \cdot \dot{x} + (K - K_{HIS}) \cdot x = F_w$$

5.3.1 Stiffness matrix K_{HIS}

The cross-sectional area of different cylinders can be expressed as the cross-sectional area ratio between the bottom and top of the front or rear cylinder η_i ($i = f, r$) and the ratio between the rear and front top cylinders μ are introduced, which can be written as $\eta_i = S_{iB}/S_{iT}$ and $\mu = S_{fT}/S_{rT}$.

The stiffness matrix of HIS suspension can be expressed as:

$$K_{HIS(8 \times 8)} = \frac{1}{C_p + C_a} \begin{bmatrix} \mathbf{0}_{(1 \times 1)} & \mathbf{0}_{(1 \times 3)} & \mathbf{0}_{(1 \times 4)} \\ \mathbf{0}_{(3 \times 1)} & K_{b(3 \times 3)} & K_{bw(3 \times 4)} \\ \mathbf{0}_{(4 \times 1)} & K_{bw^T(4 \times 3)} & K_w(4 \times 4) \end{bmatrix} S_{rT}^2$$

Where,

$$K_b = \begin{bmatrix} 2[(\mu - \eta_r)^2 + (\mu \eta_f)^2] & -2[(a\mu + b\eta_r)(\mu - \eta_r) + \mu \eta_f(a\mu \eta_f + b)] & 0 \\ -2[(a\mu + b\eta_r)(\mu - \eta_r) + \mu \eta_f(a\mu \eta_f + b)] & 2[(\mu - \eta_r)^2 + (\mu \eta_f)^2] & 0 \\ 0 & 0 & 2[(l\mu + l\eta_r)^2 + (l\mu \eta_f + l)^2] \end{bmatrix}$$

$$K_{bw} = \begin{bmatrix} -\mu(\mu - \eta_r) - (\mu \eta_f)^2 & -\mu(\mu - \eta_r) - (\mu \eta_f)^2 & \eta_r(\mu - \eta_r) + \mu \eta_f & \eta_r(\mu - \eta_r) + \mu \eta_f \\ \mu(a\mu + b\eta_r) + \mu \eta_f(a\mu + b\eta_r) & \mu(a\mu + b\eta_r) + \mu \eta_f(a\mu + b\eta_r) & -\eta_f(a\mu + b\eta_r) - (a\mu \eta_f + b) & -\eta_f(a\mu + b\eta_r) - (a\mu \eta_f + b) \\ -\mu(l\mu + l\eta_r) - \mu \eta_f(l\mu \eta_f + l) & \mu(l\mu + l\eta_r) + \mu \eta_f(l\mu \eta_f + l) & -\eta_r(l\mu + l\eta_r) - (l\mu \eta_f + l) & \eta_r(l\mu + l\eta_r) + (l\mu \eta_f + l) \end{bmatrix}$$

$$K_w = \begin{bmatrix} \mu^2(\eta_f^2 + 1) & 0 & 0 & -\mu(\eta_r + \eta_f) \\ 0 & \mu^2(\eta_f^2 + 1) & -\mu(\eta_r + \eta_f) & 0 \\ 0 & -\mu(\eta_r + \eta_f) & \eta_f^2 + 1 & 0 \\ -\mu(\eta_r + \eta_f) & 0 & 0 & \eta_f^2 + 1 \end{bmatrix}$$

5.3.2 Damping matrix C_{HIS}

The damping matrix of HIS suspension can be expressed as:

$$C_{HIS(8 \times 8)} = Z_A \begin{bmatrix} 0_{(1 \times 1)} & 0_{(1 \times 3)} & 0_{(1 \times 4)} \\ 0_{(3 \times 1)} & K_{b(3 \times 3)} & K_{bw(3 \times 4)} \\ 0_{(4 \times 1)} & K_{bw(4 \times 3)}^T & K_{w(4 \times 4)} \end{bmatrix} S_{rT}^2 + Z_H \begin{bmatrix} 0_{(1 \times 1)} & 0_{(1 \times 3)} & 0_{(1 \times 4)} \\ 0_{(3 \times 1)} & C_{b0(3 \times 3)} & C_{bw0(3 \times 4)} \\ 0_{(4 \times 1)} & C_{bw0(4 \times 3)}^T & C_{w0(4 \times 4)} \end{bmatrix} S_{rT}^2 + Z_R \begin{bmatrix} 0_{(1 \times 1)} & 0_{(1 \times 3)} & 0_{(1 \times 4)} \\ 0_{(3 \times 1)} & C_{b2(3 \times 3)} & C_{bw2(3 \times 4)} \\ 0_{(4 \times 1)} & C_{bw2(4 \times 3)}^T & C_{w2(4 \times 4)} \end{bmatrix} S_{rT}^2$$

$$C_{bi} = \begin{bmatrix} 2(\mu^2 \eta_f^i + \eta_r^i) & -2(a\mu^2 \eta_f^i - b\eta_r^i) & 0 \\ -2(a\mu^2 \eta_f^i - b\eta_r^i) & 2(a^2 \mu^2 \eta_f^i + b\eta_r^i) & 0 \\ 0 & 0 & 2(l^2 \mu^2 \eta_f^i + l^2 \eta_r^i) \end{bmatrix}$$

$$C_{bwi} = \begin{bmatrix} -\eta_f^i \mu^2 & -\eta_f^i \mu^2 & -\eta_r^i & -\eta_r^i \\ -a\eta_f^i \mu^2 & -a\eta_f^i \mu^2 & -b\eta_r^i & -b\eta_r^i \\ -l\eta_f^i \mu^2 & l\eta_f^i \mu^2 & -l\eta_r^i & l\eta_r^i \end{bmatrix} \quad C_{bwi} = \begin{bmatrix} \eta_f^i \mu^2 & 0 & 0 & 0 \\ 0 & \eta_f^i \mu^2 & 0 & 0 \\ 0 & 0 & \eta_r^i & 0 \\ 0 & 0 & 0 & \eta_r^i \end{bmatrix}$$

In those equations, $i = 0, 2$.

5.4 Optimize the Parameters of HIS System for the Ambulance Model

To further improve the comfort performance of the ambulance, the cross sectional ratios μ and η_i of HIS subsystem needs to be properly chosen. To do that, we build the integrated model in Matlab/Simulink, and use grade C random road profile as our road excitation and run the simulation to have the responses of acceleration of z_b , z_s , pitch and roll motion in time domain.

During the simulations, the series of different μ and η_i values are tested and the RMS values of responses of acceleration of z_b , z_s , pitch and roll motion is used as the indicators of the comfort performance of the ambulance. From the results of the RMS values, and make a trade-off between each indicators and choose the proper values of μ and η_i to achieve an overall optimal performance of the ambulance. Then, based on the optimized μ and η_i , the optimized responses of the ambulance ride performance is simulated.

5.4.1 Indicators of comfort performance of the ambulance

Patients lying inside the ambulance are particularly sensitive to even tiny intensity of vibration, acceleration of z_b is certainly one important indicator. When the ambulances are in operation, vibration in the lateral direction, due to the curves,

would make the emergency care not easy to operate for the paramedic and even cause trauma to patient. So acceleration of z_s and roll motion are also two important indicators. Moreover, the subsequent pitch motion due to frequently brake and start will generate negative foot-to-head acceleration in the lying patient, which would result in side effect, such as rapid shifting the blood to the head, reduction of venous return, and the rise of the patient's blood pressure.

In this case, there are four important indicators for the comfort performance of the ambulance: RMS of acceleration of z_b , z_s , roll of sprung mass and pitch of sprung mass.

5.4.2 Simulink model of the integrated model

The Simulink diagram of the integrated ambulance and HIS suspension model can be built shown in Figure 5.1.

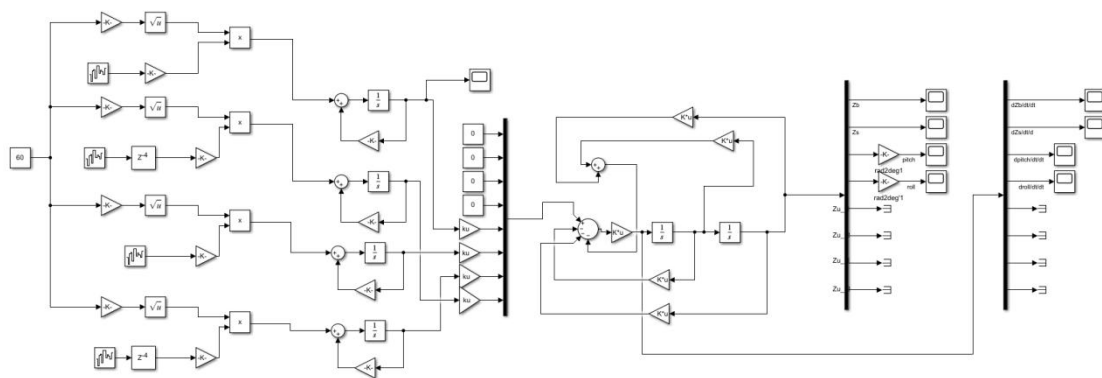


Figure 5.3 Integrated 8 DOF ambulance model with HIS suspension

5.4.3 Find the optimized value of μ

The ratio between the cross-sectional cylinder-areas of front and rear HIS μ is certainly going to influence the HIS comfort performance. To find the optimal value of μ , the results of RMS values of responses of acceleration of z_b , z_s , pitch and roll motion in time domain are shown in Figure 5.4. During this process, μ is varied from 0 to 2 at the distance of 0.1.

To find the best values of all of the three parameters μ and η_i ($i = f, r$), when varying μ , the values η_i are fixed as 1 (the right and rear cross-sectional areas of cylinders are equal).

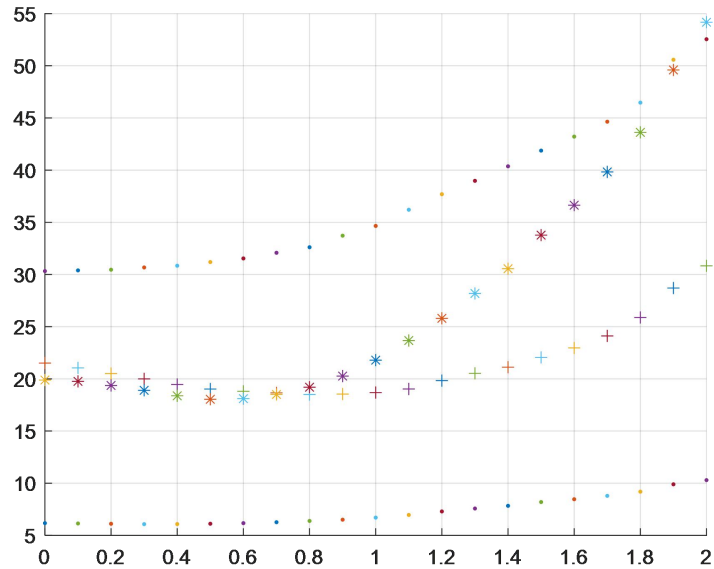


Figure 5.4 RMS values varying μ

In this figure, “+” and “*” represent the RMS values of acceleration of z_s and pitch respectively. The higher and lower “.” represent the RMS values of the acceleration of roll motion and z_b respectively.

Since lower the RMS value better the results, but from the figure we can see that there is no single certain value of μ corresponding to all four indicator. After making a trade-off, $\mu = 0.6$ can be regard as approximately the best value to achieve the overall comfort performance for the ambulance.

5.4.4 Find the optimized value of η_i

(1) The optimal value of η_f

In this process, μ is fixed at its optimal value 0.6. Then, η_f is varied from 0 to 3 at the distance of 0.1. The results of the RMS values is shown in Figure 5.5.

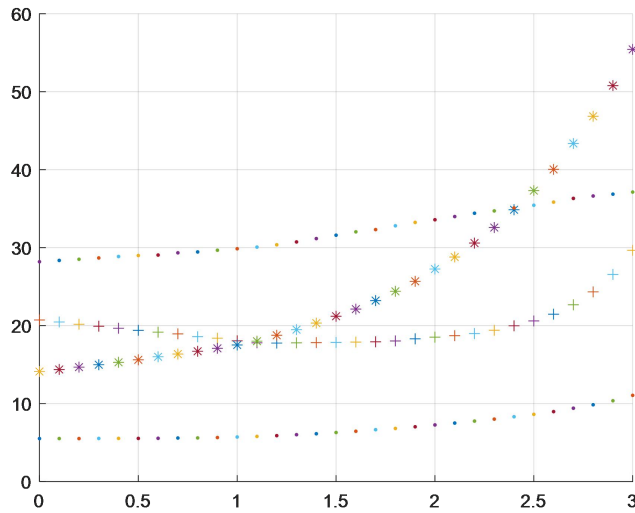


Figure 5.5 RMS values varying η_f

From the figure, the RMS of acceleration of z_s , z_b and roll is approximately the same from $\eta_f = 0$ to $\eta_f = 2$, while RMS of acceleration of pitch motion is decreasing as η_f is decreasing. So, to achieve the low RMS of pitch and at the same time not causing too high of RMS roll, the value of η_f is chosen at 0.5.

(2) The optimal value of η_r

In this process, μ and η_f are fixed at their optimal value 0.6 and 0.5. η_r is varied from 0 to 3 at the distance of 0.1. Then the results of RMS values are output in Figure 5.6.

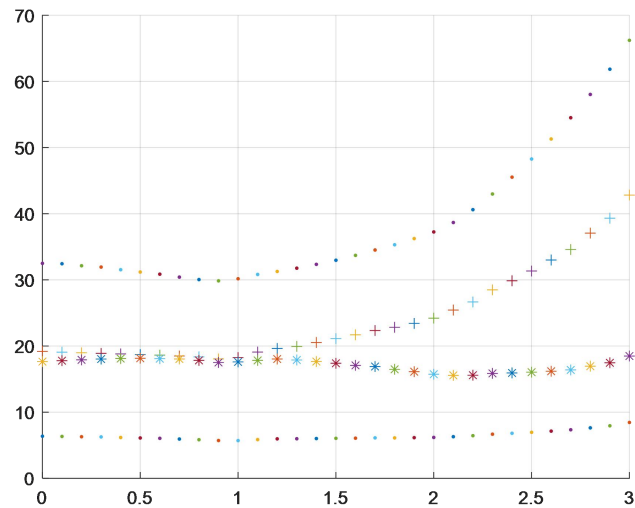


Figure 5.6 RMS values varying η_r

From the figure, the RMS of acceleration of z_s , z_b and roll is approximately constant low from $\eta_r = 0$ to $\eta_r = 1.5$, while RMS of acceleration of roll motion shows relatively obvious minimum at $\eta_r = 0.9$. So η_r is selected at value of 0.9 as its optimal one.

Summing up all the analysis, the ratio of cross-sectional areas of different cylinders are determined: $\mu = 0.6$, $\eta_f = 0.5$, $\eta_r = 0.9$.

5.5 Comparison Between HIS and Conventional Suspension

To further verify the improvement of the comfort performance of the ambulance with HIS, based on the optimal parameters of HIS ($\mu = 0.6$, $\eta_f = 0.5$, $\eta_r = 0.9$), the comfort responses of the ambulance with HIS and without HIS are compared. The input of this system is grade C random road profile. The results are shown from Figure 5.7 to 5.14.

The red line represent the responses without HIS, and the black line represent the responses with HIS.

(1) The responses of vertical motion of the stretcher

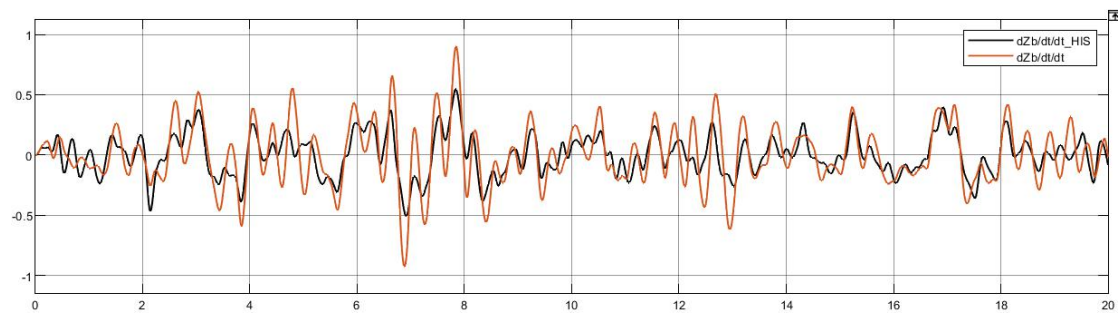


Figure 5.7 Comparison of acceleration of z_b

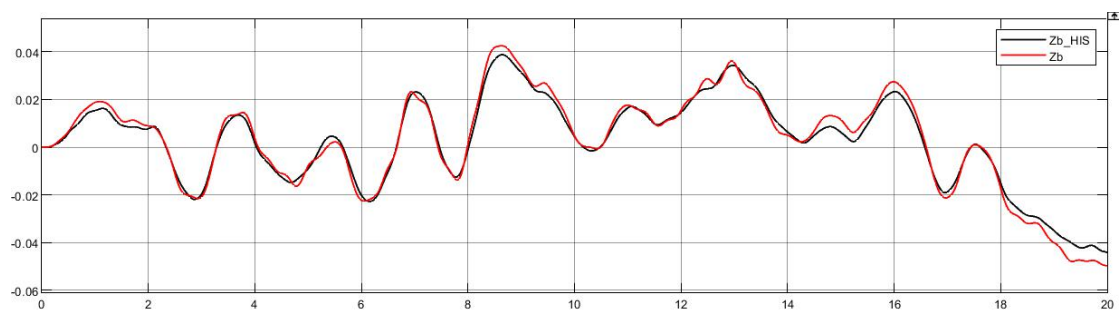


Figure 5.8 Comparison of z_b

(2) The responses of vertical motion of the sprung mass

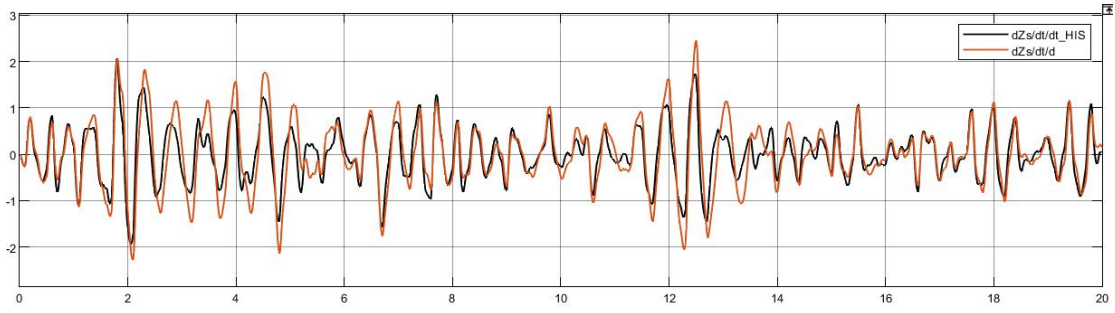


Figure 5.9 Comparison of acceleration of z_s

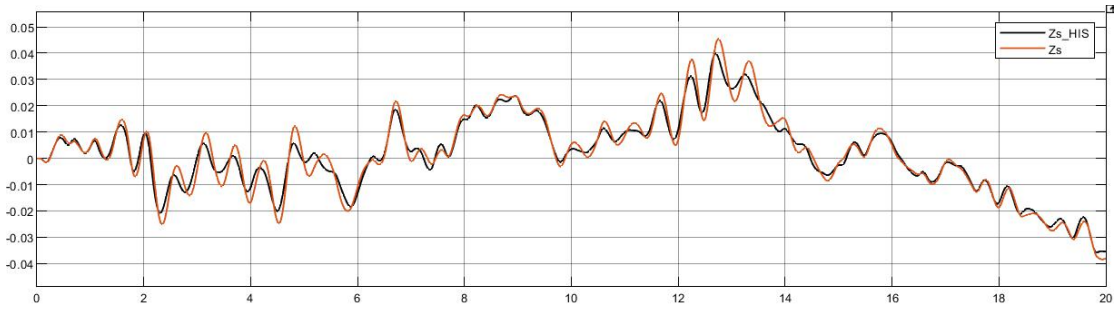


Figure 5.10 Comparison of z_s

(3) The responses of pitch motion of the sprung mass

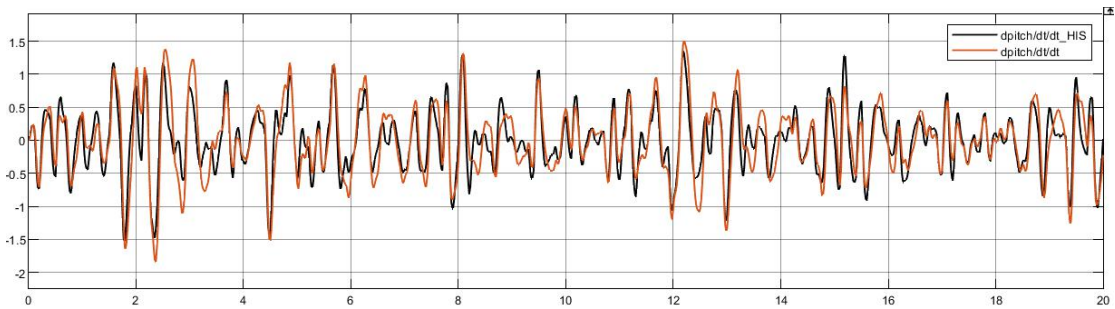


Figure 5.11 Comparison of acceleration of pitch of sprung mass

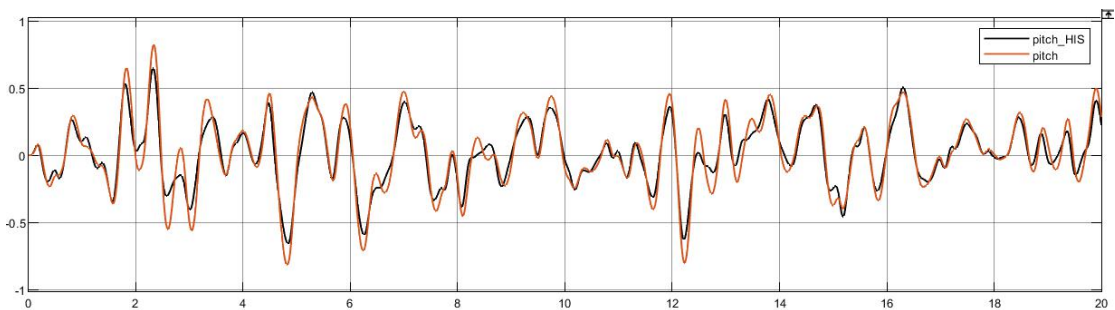


Figure 5.12 Comparison of pitch of sprung mass

(4) The responses of roll motion of the sprung mass

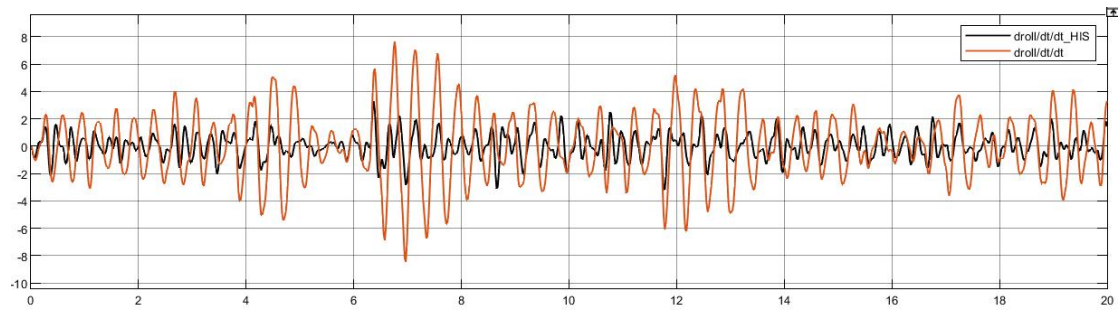


Figure 5.13 Comparison of acceleration of roll of sprung mass

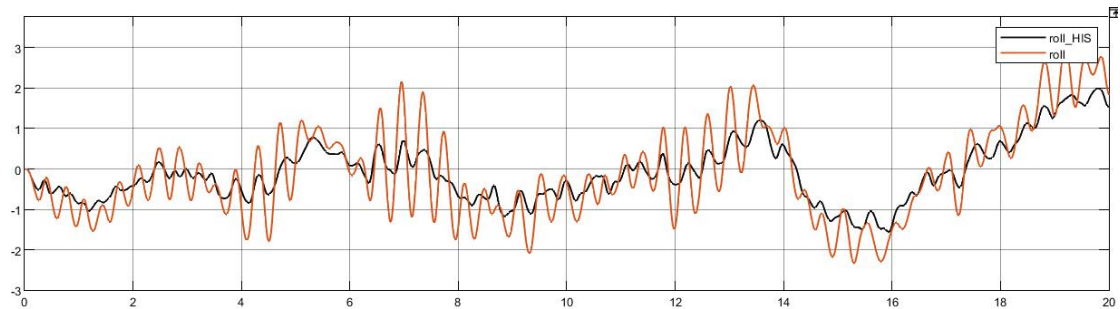


Figure 5.14 Comparison of roll of sprung mass

To show the results more clearly, the RMS values of each of the comfort responses is compared between the ambulance with and without HIS. The results are shown in the bar chart in Figure 5.15.

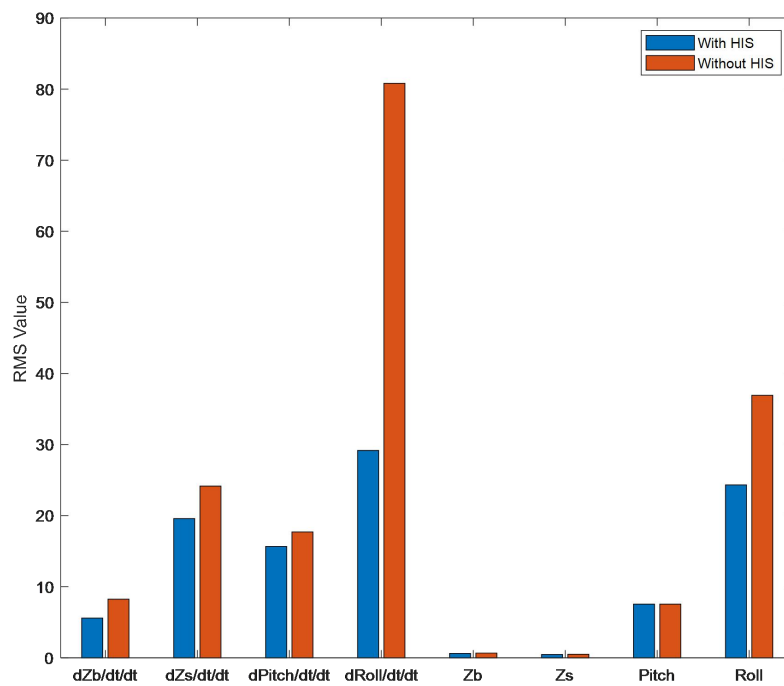


Figure 5.15 Comparison of RMS of the ambulance with and without HIS.

From this chart, we can find that the HIS can improve the comfort performance in all of these eight responses. In addition, the introduce of HIS can significantly improve the rolling performance of the ambulance. Overall, the HIS is a very good way to improve the riding performance of the ambulance.

Chapter 6

Conclusion

In conclusion, the aim of this thesis is to optimizing the comfort performance of the ambulance by using mathematical method. Start from the 7 DOF standard truck model, the thesis verifies the accuracy of the method of mathematical modeling by comparing the mathematical simulation results to Trucksim experimental results.

Based on this method of mathematical model, the thesis forward the analyse to 8 DOF ambulance model, which is the main topic of the thesis. Based on this 8 DOF, the controlled variables are accelerations of vertical motions of the stretcher and patients. And the optimized parameters are stiffness and damping value of the stretcher suspension. After choosing the optimized parameters, the comfort performance of the lying patient is largely improved. In addition, since during the riding ambulance, the speed of the ambulance is frequently changed and the road profile of the ambulance is also varied and sometimes unpredictable. Will these factors influence the optimized value of our parameters? To find out, the RMS values of the acceleration of vertical motion of the patient is used as the indicator of comfort. By varying the parameters of stiffness and damping of stretcher suspension at each different speed and road profile of the ambulance, the result is that despite all of these different conditions, the optimal parameters are independent.

However, the problem of this optimization is that only the comfort of the patient is improved, because the stretcher suspension is much soft than suspension of the sprung mass, so the comfort performance of the paramedics are rarely influenced. To fix that, in the fifth chapter, the thesis focus on properly design the ambulance suspension. In this case, a HIS subsystem is added to the conventional suspension forming an integrated HIS ambulance model. By simulating the comfort response of this integrated model and compared them with the conventional suspension obtained before, the results is that not only the comfort of the patient is improved but also the comfort performance of the sprung mass, which make it more convenient for the paramedics to perform the medical operation. What needs to be mention is that, the roll motion of the ambulance is the most optimized variable. This information can

dedicate that HIS ambulance also have a potential of improving the handling performance of the ambulance during cornering.

Bibliography

- [1] Menon V. A. Product Development Approach for a Stabilized Ambulance Stretcher. Master's Thesis, 2018.
- [2] Raemaekers A. Active Vibration Isolator Design for Ambulance Patients. Master's Thesis, Eindhoven University of Technology, Eindhoven, Holland, 2009.
- [3] Marques L., Malvezzi F., Stavropoulos K. D. Analysis of movements and degrees of freedom required for a vibration attenuation system on ambulance stretchers. *Vibroengineering Procedia*, Vol. 32, 2020, p. 81-86.
- [4] M.A. Abdelkareem, L. Xu, J. Zou, M.K.A. Ali, F. Essa, A. Elagouz, et al., Energy-harvesting potential and vehicle dynamics conflict analysis under harmonic and random road excitations, 2018. <https://doi.org/10.4271/2018-01-0568>.
- [5] Sharma S. K., Pare V., Chouksey M., Rawal B. R. Numerical studies using full car model for combined primary and cabin suspension. *Procedia Technology*, Vol. 23, 2016, p. 171-178.
- [6] Sim K., Lee H., Yoon J. W., Choi C., Hwang S.-H. Effectiveness evaluation of hydro-pneumatic and semi-active cab suspension for the improvement of ride comfort of agricultural tractors. *Journal of Terramechanics*, Vol. 69, 2017, p. 23-32.
- [7] Syabillah Sulaiman, Pakharuddin Mohd, Hishamuddin Jamaluddin, Roslan Abd, Mohammad Safwan. Modeling and validation of 7-DOF ride model for heavy vehicle. Sulaiman, 2012, ModelingAV.
- [8] Malvezzi Fernando, Maia Matarazzo Orsino Renato, Dimitriou Stavropoulos Konstantinos Parameter optimization for a vibration attenuation system on ambulance stretchers. *Vibroengineering PROCEDIA*, Vol. 37, 2021, p. 36-41.
- [9] Tan B, Wu Y, Zhang N, Zhang B, Chen Y. Improvement of ride quality for patient lying in ambulance with a new hydro-pneumatic suspension. *Advances in Mechanical Engineering*. April 2019. doi:10.1177/1687814019837804